Functional Mature Human Microglia Developed in Human iPSC Microglial Chimeric Mouse Brain

Ranjie Xu [1], Andrew J. Boreland [1], Xiaoxi Li [1], Anthony Posyton[1], Kelvin Kwan[1], Ronald P. Hart[1], Peng Jiang[1,*]

[1]Department of Cell Biology and Neuroscience, Rutgers University, Piscataway, NJ 08854, USA.

*Address correspondence to:
Peng Jiang, Ph.D.
Assistant Professor
Department of Cell Biology and Neuroscience
Rutgers University
604 Allison Road, Piscataway, NJ 08854
Email: peng.jiang@rutgers.edu
Phone: 848-445-2805

Abstract

Microglia, the brain-resident macrophages, exhibit highly dynamic functions in neurodevelopment and neurodegeneration. Human microglia possess unique features as compared to mouse microglia, but our understanding of human microglial functions is largely limited by an inability to obtain human microglia under homeostatic states. We developed a human pluripotent stem cell (hPSC)-based microglial chimeric mouse brain model by transplanting hPSC-derived primitive macrophage precursors into neonatal mouse brains. The engrafted human microglia widely disperse in the brain and replace mouse microglia in corpus callosum at 6 months post-transplantation. Single-cell RNA-sequencing of the microglial chimeric mouse brains reveals that xenografted hPSC-derived microglia largely retain human microglial identity, as they exhibit signature gene expression patterns consistent with physiological human microglia and recapitulate heterogeneity of adult human microglia. Importantly, the engrafted hPSC-derived microglia exhibit dynamic response to cuprizone-induced demyelination and species-specific transcriptomic differences in the expression of neurological disease-risk genes in microglia. This model will serve as a novel tool to study the role of human microglia in brain development and degeneration.

Introduction

As the resident macrophages of the central nervous system (CNS), microglia play critical roles in maintenance of CNS homeostasis and regulation of a broad range of neuronal responses [1, 2]. Recent studies indicate that dysfunction of microglia contributes to neurodevelopmental and neurodegenerative diseases, including Alzheimer's disease (AD) [3-7]. Moreover, genome-wide association studies have shown that many neurological disease risk genes, particularly neurodegenerative diseases, are highly and sometimes exclusively expressed by microglia [8-10]. These observations provide a compelling incentive to investigate the role of microglia in models of abnormal brain development and neurodegeneration. Most studies of microglia largely rely on rodent microglia. However, there is increasing evidence that rodent microglia are not able to faithfully mirror the biology of human microglia [11]. In particular, recent transcriptomic studies have clearly demonstrated that a number of immune genes, not identified as part of the mouse microglial signature, were abundantly expressed in human microglia [8, 12]. Moreover, a limited overlap was observed in microglial genes regulated during aging and neurodegeneration between mice and humans, indicating that human and mouse microglia age differently under normal and diseased conditions [12, 13]. These findings argue for the development of species-specific research tools to investigate microglial functions in human brain development, aging, and neurodegeneration.

Functional human brain tissue is scarcely available. In addition, given the considerable sensitivity of microglia to environmental changes [8], the properties of available human microglia isolated from surgically resected brain tissue may vary significantly, due to different disease states of the patients and the multi-step procedures used for microglial purification. In order to study human microglia in a relatively homeostatic state, many scientists have turned to human pluripotent stem cells (hPSCs). Recent advances in stem cell technology have led to the efficient generation of microglia from hPSCs [14-19], providing an unlimited source of human microglia to study their function. However, when cultured alone or co-cultured with neurons and astrocytes in 2-dimensional (2D) or 3D organoid/spheroid culture systems, these hPSC-derived microglia best resemble fetal or early postnatal human microglia. This is indicated by much lower expression of key microglial molecules such as TREM2, TMEM119, and P2RY12 in the hPSC-derived microglia, as compared to microglia derived from adult human brain tissue [16, 18, 20]. Thus, even with these novel *in vitro* models, it has been challenging to advance understanding of human microglial function in adult ages or in neurodegeneration during aging.

Recent studies from us [21, 22] and others [23-25] have demonstrated that neonatally engrafted human neural or macroglial (oligodendroglial and astroglial) progenitor cells can largely repopulate and functionally integrate into the adult host rodent brain or spinal cord, generating widespread chimerism. This human-mouse chimeric approach provides unique opportunities for studying the pathophysiology of the human cells within an intact brain. In this study, we developed a hPSC microglial chimeric mouse brain model, by transplanting hPSC-derived microglia into neonatal mouse brains. The engrafted hPSC-derived microglia can proliferate, migrate, and widely disperse in the brain. We hypothesize that the limited functional maturation of hPSC-derived microglia in *in vitro* models is primarily caused by the fact that those microglia are maintained in an environment that lacks the complex cell-cell/cell-matrix interactions existing in an *in vivo* brain environment [8]. To test this hypothesis, we employed single-cell RNA-sequencing and super-resolution confocal imaging to examine the identity and function of hPSC-derived microglia developed for six months in the mouse brain under both homeostatic and toxin-induced demyelination conditions.

Results

Generation of hPSC microglial chimeric mouse brains

Microglia originate from yolk sac erythromyeloid progenitors (EMPs) during primitive hematopoiesis. EMPs further develop to primitive macrophage precursors (PMPs) that migrate into the developing neural tube and become microglia with ramified processes within the CNS environment [1]. We first derived PMPs from hPSCs, including one human induced pluripotent stem cell (hiPSC) line and one human embryonic stem cell (hESC) line, using a published protocol [18]. Briefly, the yolk sac embryoid bodies (YS-EBs) were generated by treating the EBs with bone morphogenetic protein 4 (BMP4), vascular endothelial growth factor (VEGF), and stem cell factor (SCF). Next, the YS-EBs were plated into dishes with interleukin-3 (IL-3) and macrophage colony-stimulating factor (M-CSF) to promote myeloid differentiation. At 2–3 weeks after plating, hPSC-derived PMPs emerged into the supernatant and were continuously produced for more than 3 months. The cumulative yield of PMPs was around 40-fold higher than the number of input hPSCs (Figure 1A), similar to the results from previous studies [16, 18, 26]. PMPs are produced in a Myb-independent manner that closely recapitulated primitive hematopoiesis [1, 18, 27]. We confirmed the identity of these hPSC-derived PMPs by staining with CD235, a marker for YS primitive hematopoietic progenitors [28, 29], and CD43, a marker for hematopoietic progenitor-like cells[28, 29]. As shown in Figure 1B, over 95% of the hPSC-derived PMPs expressed both markers. Moreover, the human PMPs are highly proliferative as indicated by Ki67 staining (95.4 ± 2.2%, n = 4) (Figure 1B). Using this method, we routinely obtain ample numbers of hPSC-derived PMPs with high purity as required for cell transplantation experiments.

We engrafted hPSC-derived PMPs into the brains of postnatal day 0 (P0) immunodeficient mice that are Rag2/IL2rγ-deficient and also express the human forms of CSF1, which facilitates the survival of xenografted human myeloid cells and other leukocytes[30, 31]. We deposited cells into the white matter overlying the hippocampus and sites within the hippocampal formation (Figure 1C). In order to visualize the distribution of donor-derived microglia, at 6 months post-transplantation, we stained the mouse brain sections with human-specific antibody recognizing TMEM119 (hTMEM119). TMEM119 is a marker that is only expressed by microglia, but not other macrophages [14, 17, 32]. We found that the donor-derived hTMEM119$^+$ microglia widely disperse in the brain (Figure 1D). As early as 3 weeks post-transplantation, donor-derived microglia had already migrated along corpus callosum and passed through the rostral migratory stream to the olfactory bulb (Figure 1E). At 6 months post-transplantation, human microglia widely dispersed in multiple brain regions, including olfactory bulb, hippocampus, and cerebral cortex, and exhibited a highly ramified morphology (Figure 1F and G). Frequently, we also observed clusters of human microglia in the cerebellum (Figure 1H), which might be a result from the strong ability of immune cells trafficking along blood vessels and/or the choroid plexus [33]. Similar to our previous studies [24, 25], we assessed the engraftment efficiency and degree of chimerization by quantifying the percentage of hTMEM119$^+$ cells among total DAPI$^+$ cells in the forebrain in sagittal brain sections covering regions from 0.3 to 2.4 mm lateral to midline and found that about 8% of the total cells were human microglia in the 6-month-old mouse brains (Figure 1D and L). As shown by individual data points overlaid on the bar graphs (Figure 1L), there were variations in chimerization among animals. In addition to the images showing distribution of donor-derived cells in Figure 1D, we thus also included tile scan images collected from another chimeric mouse brain that represents the lower level of chimerization (supplementary Figure 1A). In the developing brain, microglia are known to use white matter tracts as guiding structures for migration and that they enter different brain regions [34]. In order to examine the migration pattern of our transplanted cells, we deposited PMPs into different sites, the lateral ventricles of P0 mice. As early as three weeks post-transplantation, we found that the majority of donor-derived cells migrated along the anterior corpus callosum, rostral migration stream, and then entered the olfactory bulb. Moreover, some of those cells of migrated posteriorly along the corpus callosum (supplementary Figure 1B), suggesting that engrafted cells likely used corpus callosum to migrate to various brain regions. These results demonstrate that hPSC-derived PMPs survive in mouse brain and that they migrate to a variety of structures.

To examine whether transplanted hPSC-derived PMPs efficiently differentiated to microglia in the mouse brain, we double-stained brain sections for both human nuclei (hN) and hTMEM119. As early as 8 weeks post-transplantation, the vast majority of hN^+ donor-derived cells (93.2 ± 2.2%, n =7) were positive for hTMEM119 (Figure 1I and M), indicating the robust and efficient differentiation of hPSC-derived PMPs into microglia. Moreover, the vast majority of the donor-derived cells expressed PU.1, a transcription factor that is necessary for microglial differentiation and maintenance[35-38], and were positive for human specific CD45 (hCD45), which is expressed by all nucleated hematopoietic cells (Figure 1J) [39, 40]. Similarly, at 6 months post-transplantation, the vast majority of donor-derived cells expressed hTMEM119 (supplementary Figure 2A) and P2RY12 (93.4 ± 3.8%, n = 7; supplementary Figure 2B and C). hTMEM119 and P2RY12 was not expressed in PMP cultures (supplementary Figure 2D). Moreover, we examined the distribution of human donor cells in border regions, including choroid plexus, meninges, and perivascular spaces. We found that most of the $hTMEM119^-/hN^+$ donor-derived cells were seen in those border regions. Furthermore, we co-stained hTMEM119 with CD163, an established marker for non-microglial CNS myeloid cells [41, 42]. In choroid plexus, we found that some of the $hTMEM119^-$ cells co-expressed CD163, suggesting that these transplanted cells differentiated into choroid plexus macrophage (cpMΦ), but not microglia (supplementary Figure 3A). In order to better visualize meninges and perivascular space, we triple-stained hN and CD163 with laminin, a marker that has been commonly used to visualize vascular structures in the mammalian brain [43]. There was also a small number of hN^+ and $CD163^+$ co-expressing cells in these regions, indicating that the transplanted cells differentiated into meningeal macrophage (mMΦ) and perivascular macrophages (pvMΦ) (supplementary Figure 3B and C). There was a possibility that some transplanted cells might remain as progenitors and maintain their hematopoietic progenitor-like cell identity. As shown in supplementary Figure 3D, we found that a small population of hN^+ cells expressed CD235 in the regions close to the lateral ventricles. Overall, these results demonstrate that the vast majority of engrated hiPSC-derived PMPs differentiate into $hTMEM119^+$ microglia, with a relatively small number giving rise to other of $hTMEM119^-$ CNS myeloid cells in a brain context-dependent manner or remaining as progenitors.

We next assessed the proliferation of engrafted cells by staining the proliferative marker Ki67. As shown in Figure 1K and N, at 3 weeks post-transplantation, about 17% (16.9 ± 5.7%, n = 8) of hN^+ transplanted cells expressed Ki67, indicating that these cells were capable of proliferating in the mouse brain. At 6 months post-transplantation, the percentage of proliferating cells dramatically decreased and less than 2% (1.7 ± 0.8%, n = 7) of total engrafted cells were Ki67 positive. These $Ki67^+$ proliferating human cells mainly localized in the subventricular zone, the walls along lateral ventricles, corpus callosum, and olfactory bulb (Figure 1K and supplementary Figure 3E). We also examined the proliferation of mouse host microglia at different brain regions at 3 weeks post-transplantation. We only found a very small number of $Ki67^+$ mouse microglia in the subventricular zone (supplementary Figure 3F), which is consistent with a previous report [44]. Taken together, these findings demonstrate that engrafted hPSC-derive PMPs differentiate to microglia, generating a mouse brain with a high degree of human microglial chimerism in the forebrain.

Human PSC-derived microglia undergo morphological maturation and are functional in the mouse brain

Compared with three weeks post-transplantation, hPSCs-derived microglia appeared to exhibit more complex processes at 6 months post-transplantation (Figure 1E and F). Moreover, even at the same stage, hPSC-derived microglia in the cerebral cortex seemed to exhibit much more complex morphology, compared with the hPSCs-derived microglia in the corpus callosum and cerebellum (Figure 1G and H and hTMEM119 and Iba1 staining in supplementary Figure 2A and 4, respectively). In the corpus callosum, hPSC-derived microglia had fewer branches that aligned with axons; and in the cerebral cortex, the microglia exhibited more complex and ramified processes (supplementary Figure 2A and 4), similar to observations from previous studies [34, 45]. This prompted us to further examine the morphological and functional changes of the hPSC-derived microglia along with the development of the

mouse brain, particularly in cerebral cortex. Previous studies have shown that there are no changes in microglial number, cytokine levels, and gene expression profiles between wild type and *Rag2*$^{-/-}$ mice [46]. Building upon that, we also compared the differences between xenografted hPSC-derived microglia vs. host mouse microglia. We double-stained the brain sections with human and mouse specific TMEM119 (hTMEM119 and mTMEM119, respectively) antibodies to distinguish hPSC-derived microglia and mouse host microglia (Figure 2 A and B). As shown in Figure 2A, in 6 month old mice, both hPSCs-derived microglia and mouse microglia were seen in the cerebral cortex and hippocampus. Notably, we observed that mouse microglia mainly resided in distal regions in the cerebral cortex and hippocampus. In particular, in the corpus callosum, mouse microglia were rarely seen, and the vast majority of microglia were hPSC-derived microglia (Figure 2C), indicating that hPSC-derived microglia replaced the host mouse microglia. In the cerebral cortex, hTMEM119^{+} hPSC-derived microglia exhibited much more complex processes at 8 weeks and 6 months post-transplantation than those cells at 3 weeks post-transplantation, as indicated by the increased number of endpoints (Figure 2D). The total length of processes of hPSC-derived microglia also significantly increased from week 3 to week 8 and month 6 (Figure 2E), suggesting the gradual maturation of hPSC-derived microglia in mouse brain. We further examined the morphological differences between hPSC-derived microglia vs. mouse microglia at the same time points after transplantation. In the cerebral cortex, at 3 weeks post transplantation, compared with hPSC-derived microglia, mouse microglia showed a significantly higher number of endpoints and a slight trend of longer processes (Figure 2D and E). However, at 8 weeks post-transplantation, there was no significant difference in endpoint number and process length between hPSC-derived microglia and mouse microglia (Figure 2D and E). Interestingly, at 6 months post-transplantation, hPSC-derived microglia exhibited a significantly higher number of endpoints and longer process length than mouse microglia. Since microglial morphology is inextricably linked to their phagocytic functions [47, 48], we examined the expression of CD68, a marker for the phagolysosome [49, 50]. In the cerebral cortex, CD68 was expressed in some of the hPSC-derived microglia at 3 weeks post-transplantation and its expression dramatically decreased from 8 weeks to 6 months post-transplantation (Figure 2F and G). We observed some hTMEM119^{-}/CD68^{+} cells at 3 weeks and nearly no hTMEM119^{-}/CD68^{+} cells at 6 months post-transplantation (Figure 2G), suggesting that nearly no host mouse microglia expressed CD68 at 6 months post-transplantation. Taken together, hPSC-derived microglia show variable morphologies in a spatiotemporal manner and morphologically differ from the host mouse microglia.

Microglia have been shown to shape synapse formation by pruning synapses and to maintain oligodendroglial homeostasis by phagocytizing oligodendroglial cells [51-53]. We therefore investigated whether hPSCs-derived microglia are functional in the mouse brain. To examine synaptic pruning function, we employed a super-resolution imaging technique to visualize synapse engulfment by hPSCs-derived microglia. We triple-stained hTMEM119 with both a post-synaptic marker PSD95 and a pre-synaptic marker synapsin I. The 3D reconstruction images show that PSD95^{+} and synapsin I^{+} puncta are colocalized within hTMEM119^{+} processes, indicating that these synaptic proteins are phagocytosed by hPSCs-derived microglia at eight weeks post-transplantation in grey matter **(**Figure 3A**).** In addition, we also validated the specificity of PDS95 puncta staining by incubating brain sections with the PSD95 antibody together with a PSD95 peptide. We barely detected any PSD95^{+} puncta signal after the incubation in the presence of PSD95 peptide (supplementary Figure 5A)**.** We also triple-staining hTMEM119 and PSD95 with CD68. As shown in Figure 3B and supplementary Figures 5B, 5C**,** PSD95^{+} puncta are localized within CD68^{+} phagolysosomes in hTMEM119^{+} hPSCs-derived microglia, further indicating their synaptic pruning function. Of note, this engulfment of synaptic materials was observed from 3 weeks to 6 months post-transplantation, with a peak at 8 weeks post-transplantation (Figure 3C). Very few mouse microglia were found to engulf synaptic proteins at 8 weeks post-transplantation (supplementary Figure 6A). To examine the function of phagocytosing oligodendroglia, we double-stained hCD45 with PDGFRα, a marker for oligodendroglial progenitor cell. We observed that hCD45^{+} human microglia were able to engulf PDGFRα^{+} oligodendroglia at 3 weeks post-transplantation in the corpus callosum (Figure 3D). We also double stained hCD45 with the

oligodendroglial marker OLIG2 and similarly found that hPSCs-derived microglia in white matter engulfed OLIG2$^+$ oligodendroglia at 3 weeks post-transplantation (supplementary Figure 6B). In addition, we detected that a small population of mouse microglia engulfed OLIG2$^+$ oligodendroglia in the corpus callosum at 3 weeks post-transplantation (supplementary Figure 6C).

Microglia, together with endothelial cells, pericytes and astrocytes, form the functional blood–brain barrier [54-56]. We double-stained brain sections with hCD45 and laminin. We found that hPSC-derived microglia clustered around and were closely affiliated with laminin$^+$ blood vessels in both grey matter and white matter across different brain regions including the olfactory bulb (Figure 3E and supplementary Figure 6D). In addition, we also found that mouse microglia similarly had close contact with blood vessels in the cerebral cortex, corpus callosum, and olfactory bulb (supplementary Figure 6E). Altogether, these results demonstrate hPSCs-derived are functional in the mouse brain under homeostatic conditions. The human microglia and host mouse microglia exhibited similar microglial functions, including synaptic pruning, phagocytosis of oligodendroglia, and having contact with blood vessels.

Single-cell RNA-sequencing of hiPSC microglial chimeric mouse brain identifies a gene expression signature consistent with adult human microglia

Homeostatic human microglia at adult stages are difficult to obtain, because microglia are highly sensitive to environmental changes and microglia derived from adult human brain tissue-derived are usually purified through multi-step procedures that can change their biological properties significantly [8]. In addition, microglia derived from hPSCs using all current differentiation protocols largely resemble fetal or early postnatal human microglia[16, 18, 20]. We hypothesize that hPSC microglial chimeric mice may provide a unique opportunity to study biological properties of adult human microglia, because the engrafted hPSC-derived microglia are likely to exhibit an expedited maturation process promoted by the maturing environment in the mouse brain. To test this hypothesis, we examined transcriptomic profiles of hiPSC-derived microglia, developed in the *in vivo* homeostatic mouse environment, using single-cell RNA-sequencing (scRNA-seq). We collected brain regions where engrafted hiPSCs-derived microglia preferentially dispersed, including the cerebral cortex, hippocampus, corpus callosum, and olfactory bulb, from 6-month-old chimeric mouse brain for scRNA-seq. A previous study has demonstrated that within hours during which microglia are isolated from the brain environment and transferred to culture conditions, microglia undergo significant changes in gene expression [8]. To capture observed expression patterns as close to the “in vivo” patterns as possible, we chose to omit a FACS sorting step since it would have added substantial processing time. Owing to the wide distribution and high abundance of hiPSC-derived microglia in those brain regions, we were able to capture ample numbers of hiPSC-derived microglia for scRNA-seq even without enrichment by FACS sorting. After brain tissue dissociation with papain and centrifugation to remove debris and myelin, single cell suspensions were directly subjected to droplet-based 10X Genomic RNA-seq isolation (Fig. 4A). Using stringent criteria, 29,974 cells passed the quality control evaluation (with about 10,000–15,000 reads/cell) from 4 animals for downstream analysis (supplementary Figure 7A).

We performed dimensionality reduction and clustering using a principal component analysis (PCA)-based approach. Using t-distributed stochastic neighbor embedding (t-SNE) to visualize cell clustering, we identified 11 clusters, including a cluster of xenografted hiPSC-derived microglia, which we named Xeno MG (Fig. 4B). This clustering pattern was consistently and independently obtained in all four animals, indicating the reproducibility of the sequencing and clustering procedures (supplementary Figure 7B). We defined each cluster based on the expression of enriched genes (Table S1) that could be recognized as markers for specific cell types or are reported to be abundantly expressed in specific cell types (Figure 4C and supplementary Figure 7C). The clusters included 10 mouse cell types: astrocytes (*SCL6A11*[57], *NTSR2*[58]), oligodendrocytes (*CLDN11*[59], *CNP*[60]), oligodendrocyte progenitor cells (OPC; *PDGFRα*, *OLIG2*[61]), excitatory neurons (*SYT1*[62], *SNAP25*[63]), neuronal precursors (*SOX11*, [64], *STMN2*, [65]), vascular cells (*MYL9*[66], *MGP*[67]), choroid cells (*LCN2*[68],*1500015O10Rik*[69]), endothelial cells (*ITM2A*[70], *FLT1*[71]), GABAergic neuron (*NPY*[72], *NR2F2*[73])

and mouse microglia (*P2RY12, C1QA, and CX3CR1*). The only human cell cluster, labeled Xeno MG, similarly expressed the microglial markers *P2RY12, C1QA, and CX3CR1*, and accounted for about 7% of total cells in our selected dissected regions (supplementary Figure 7D). Of note, a cross-correlation analysis of clustered cell types showed that Xeno MG had a highest correlation coefficient value (0.776) with mouse microglia, consistent with a microglial identity of the engrafted human cells (supplementary Figure 7E). Furthermore, the expression of a set of canonical microglial genes (*C1QA*, *CX3CR*, *TREM2*, *CSF1R*, and *P2RY12*) was only detected in Xeno MG and mouse microglia clusters (Figure 4D). Moreover, we performed bulk RNA-seq to analyze the pre-engraftment hiPSC-derived PMPs. We compared transcriptomic profiles between PMPs and Xeno MG from 6 months old chimeric mice. Notably, as shown in Figure 4E, compared with PMPs, Xeno MG highly expressed microglial identity markers, such as *TMEM119*, *P2RY12*, *SALL1*, and *OLFML3*, which were barely detected in PMPs. On the other hand, the expression of markers for hematopoietic progenitor cells, such as *CD59*, *CD44*, and *CD38*, was low in Xeno MG but much higher in PMPs. Furthermore, we compared the transcriptomic profile of Xeno MG with a published dataset generated from human brain tissue-derived human microglia[12]. A significant correlation was observed between Xeno MG and the published dataset[12] (supplementary Figure 8A), further confirming the human microglial identity of the engrafted human cells. As shown in Figures 1 and 2, the highly ramified morphology of hiPSC-derived microglia suggest that they stay at a homeostatic state. We examined expression of several pro-inflammatory cytokines to assess the impact of the tissue preparation procedures on the microglial state. Consistently, we found very minor expression of acute pro-inflammatory cytokines such as IL-1β, IL-1α and TNF-α[74 75, 76] (supplementary Figure 8B). In contrast, the pro-inflammatory cytokine, IL-6 and an anti-inflammatory cytokine, IL-10, were nearly undetectable, and expression of these pro-inflammatory cytokines is often correlated with a longer-lasting inflammatory response[75, 76]. This observation suggests that only a very mild inflammatory reaction was likely triggered in the Xeno MG during sample preparation, similar to previous reports [53, 74]. These results demonstrate that Xeno MG developed in the mouse brain largely retain their human microglial identity and exhibit a gene expression pattern characteristic of homeostatic human microglia.

Next, to further evaluate identity and maturation of Xeno MG in chimeric mouse brains, we compared the global expression patterns of 21 genes including the 11 microglia-specific genes and 7 HPC-specific genes shown in Figure 4E, as well as 3 NPC genes (*NES*, *DCX*, and *SOX2*) between our Xeno MG, hiPSC-derived PMPs and published datasets of hiPSC-derived microglia cultured under 2-dimensional (2D) conditions (iPS MG)[17, 77], hiPSC-derived microglia developed in 3D cerebral organoids (oMG)[78], hiPSC-derived microglia developed in mouse brain (xMG) as reported in a recent study[12, 78]. brain-tissue derived adult human microglia, including adult ex vivo microglia (Adult MG ExVivo) from Gosselin et al., 2017[17, 77] (age from 13-17 years) and Galatro et al., 2017(age from 34-102 years) [17, 77], in vitro microglia (MG InVitro) from Gosselin et al., 2017[17, 77], as well as blood/liver macrophages [17, 77]. As shown in Figure 4F, a principal component analysis (PCA) demonstrated that Xeno MG, together with xMG, were markedly distinct from blood/liver macrophages, PMPs, and the hiPSC-derived MG cultured under 2D conditions or developed in organoids. The human microglia cultured *in vitro* were separate from the other two clusters, which might suggest the significant impact of culture conditions on gene expression in those microglia as previously reported [8]. Our Xeno MG clusters intermingled with a cluster of adult MG, suggesting their resemblance to adult human microglia. Recent unbiased hierarchical clustering analyses revealed four major subclasses of adult human microglia derived from human brain tissue [79]. To determine if Xeno MG also exhibited similar heterogeneity in chimeric mouse brain, we examined the expression of the most differentially regulated genes identified from the different subclasses of adult human microglia [79]. Gene expression analysis revealed that *CD74*, *SPP1*, *C3*, and *CST3*, which were highly expressed in all subclasses in adult human microglia, had a similarly uniform pattern of expression among most Xeno MG cells. Moreover, a chemokine gene *CCL4*, the zinc finger transcription factors *EGR1*, *EGR2* and *EGR3*, *CD83*, and *MCL1*, which are each characteristically expressed in individual subclasses of human microglia, similarly had upregulated expression in distinct subpopulations of Xeno MG (Figure 4G and

supplementary Figure 8C). Taken together, these results demonstrate that Xeno MG developed in the mouse brain highly resemble mature human microglia and faithfully recapitulate heterogeneity of adult human microglia.

Transcriptomic profiling analysis reveals differences between co-resident Xeno MG and mouse microglia

Previous studies reported differences in transcriptomic profiles between human and mouse microglia [8, 12]. In the chimeric mouse brain, as xenografted hiPSC-derived microglia and host mouse microglia developed in the same brain environment, this model may provide a unique opportunity to directly examine the differences between human and mouse microglia. Xeno MG and host mouse microglia clusters obtained from 4 independent samples of 6-month-old chimeric mouse brains were used for the following comparison (Figure 5). We first compared the average levels of microglial gene transcripts in Xeno MG with orthologous gene transcripts in host mouse microglia. Consistent with previous findings [8, 12], the comparison between Xeno MG and mouse microglial transcriptomes demonstrated similar gene expression patterns overall ($r^2 = 0.553$; $p < 2.2 \times 10^{-16}$), and the majority of orthologous genes pairs (14,488 of 15,058; 96.2%) were expressed within a twofold range (black dots, Figure 5B). Using a cut-off of 2-fold difference and an FDR of 0.05, we identified that 91 gene transcripts were preferentially expressed in human microglia, whereas 84 gene transcripts were preferentially expressed in mouse microglia (supplementary Figure 8D and Table S2). Importantly, previously-reported signature genes expressed in human microglia[8], including *SPPI*, *A2M*, and *C3*, and signature genes expressed in mouse microglia, including *HEXB*, *SPARC*, and *SERINC3*, were all differentially expressed in our sequencing data (Figure 5B and C), indicating the high fidelity of our samples in resembling previously-identified human vs. mouse microglial gene expression profiles. To explore the function of genes that were highly expressed human microglia, we further performed Gene Ontology (GO) term analysis. Many significantly enriched terms were associated with the innate immune activity of microglia, such as "immune system response," "cellular response to chemical stimulus," and "regulation of cytokine production." This finding of enriched innate immunity-related gene in our Xeno MG could be either reflect the nature of human microglia as reported previously [12, 80], or the result from differential responses to critical signals from murine molecules, such as fractalkine. These results suggest that, compared to the host mouse microglia, Xeno MG and mouse microglia exhibit overall similar patterns of transcriptomic profile, but numerous species-specific differentially expressed genes were also observed.

Previous studies have shown that several disease risk genes, such as genes associated with AD, Parkinson's disease (PD), multiple sclerosis (MS), and schizophrenia (SCZ), are preferentially expressed in microglia[8, 80, 81]. Moreover, relative expression of these genes in human and mouse microglia are also different [8]. Therefore, we examined the expression of disease risk genes in Xeno MG and mouse microglia from our chimeric mouse brain preparation. Expression of disease risk genes, as reported in a recent study [8], had a highly similar differential expression pattern in co-resident mouse and human microglia (Figure 5D, E and supplementary Figure 8F-I). Specifically, with respect to MS, we found that out of 32 MS genes, 29 genes, including *ZFP36L1*, *RPL5*, and *NDFIP1* were more abundantly expressed in Xeno MG than in mouse microglia (Figure 5D and E). Similarly, out of 14 AD genes, 10 genes including *Apoc1, Sorl2,* and *Mpzl1,* were more abundantly expressed in Xeno MG than in mouse microglia (supplementary Figure 8F and I). Out of the 20 PD genes listed in a previous report [8], 18 genes, such as *Vps13c, Snca, Fgf20, Mnnrn1*, and *Lrrk2*, had the same trend of differential expression with greater expression in Xeno MG than in mouse microglia (supplementary Figure 8H and I). We also found that some of the disease genes were preferentially expressed in mouse microglia, such as *Syt11*and *Gba* in PD. Altogether, these observations demonstrate that our hPSC microglial chimeric mouse brain can faithfully model disease-relevant transcriptomic differences between human and mouse microglia, and this new model will serve as a new tool for modeling human neurological disorders that involve dysfunction of microglia.

Human PSC-derived microglia are dynamic in response to cuprizone-induced demyelination

To explore whether Xeno MG are functionally dynamic in response to insult, we fed 3 months old chimeric mice with cuprizone-containing diet to induce demyelination. The cuprizone model is one of the most frequently used models to study the pathophysiology of myelin loss in multiple sclerosis [82]. It is appropriate to use our hiPSC microglial chimeric mouse brain to examine the dynamics of human microglia under a demyelination condition, considering our observation that a large number of Xeno MG reside in the corpus callosum at 3 to 4 months post-transplantation and Xeno MG were found nearly exclusively in the corpus callosum at 6 months post-transplantation (Figure 2C). After 4 weeks of cuprizone treatment, we found that myelin structure, indicated by MBP staining in the corpus callosum, was disrupted and became fragmented in our chimeric mice (Figures 6A), in contrast to the intact and continuous MBP^+ myelin structure in chimeric mice fed with control diet (supplementary Figure 9). As shown in the super-resolution images in Figure 6B and C, engulfment of MBP^+ myelin debris by both Xeno MG and mouse microglia were clearly seen in the corpus callosum. Notably, more myelin debris was found inside of mouse microglia, compared with Xeno MG (Figure 6D). In addition, we also examined the expression of CD74 and SPP1, which is known to be upregulated in multiple sclerosis [83]. Without cuprizone treatment, variations in CD74 expression among animals were observed in Xeno MG and on average, about 20% of Xeno MG expressed CD74 (Figure 6E and F). Nearly no Xeno MG expressed SPP1 in the corpus callosum (Figure 6G and H). With cuprizone treatment, many of the Xeno MG expressed CD74 or SPP1, recapitulating the upregulated expression of CD74 and SPP1 in MS (Figure 6E-H). In mice, CD74 and SPP1 were shown to characterize white matter-associated subsets of microglia that appear during development [53]. In our study, there was a discrepancy between the *CD74* and *SPP1* transcript levels and their protein levels. This might suggest an involvement of a sophisticated control of mRNA translation that was observed in regulation of other genes critical for brain development [84, 85]. Altogether, these results demonstrate that human Xeno MG are dynamic in response to insult in mouse brain.

Discussion

Humanized mouse models, in which the immune system is reconstituted with cells of human origin, have been well-established and provide powerful tools for studying cancer, inflammatory and infectious disease, and human hematopoiesis [86]. In this study, by engrafting neonatal mice with hPSC-derived PMPs, we demonstrate the generation of chimeric mouse brains in which hPSC-derived microglia widely disperse. We propose that the following three reasons may account for the generation of human microglial chimeric mouse brain. First, as compared to other types of neural cells, microglial cells are unique in that they turn over remarkably quickly, allowing the vast majority of the population to be renewed several times during a lifetime [87-89]. Previous studies have shown that neonatally transplanted human macroglial or neural progenitor cells can outcompete and largely replace the host mouse brain cells [21, 90, 91]. In this study, we also observe that the hPSC-derived PMPs are highly proliferative prior to transplantation and transplanted cells divide for at least 6 months in the mouse host brain. Therefore, the nature of high turnover rate of microglia and the competitive advantage of engrafted human cells over endogenous mouse cells may result in a large number of human donor-derived microglia and brain regions being repopulated by hPSC-derived microglia in the mouse brain at 6 months. Second, during early brain development, microglial cells use blood vessels and white matter tracts as guiding structures for migration and enter all brain regions [34]. Thus, transplantation of hPSC-derived PMPs to the anterior anlagen of the corpus callosum of the neonatal mouse brain in this study may facilitate migration of donor cell-derived microglia, resulting in wide dispersion of hPSC-derived microglia into different brain regions. In addition, in support of this concept, we also observe that in the mouse brain, hPSC-derived microglia are concentrated around and have close contact with blood vessels in both grey matter and white matter. Lastly, although several previous studies also transplanted hPSC-derived microglia into mouse brains, the generation of chimeric mice with a high degree of human microglial brain chimerism has not been reported [16, 92]. We propose that this might be because of the age of the host animals used for cell transplantation. Previous studies used adult animals for cell transplantation [16, 92]. In our study, we transplanted hPSC-derived PMPs into the mouse brain at the earliest postnatal age, P0, as in general the neonatal brain is more receptive for the transplanted cells and more conducive for their survival and growth [21, 24, 91]. This is also supported by a recent study in which neonatal animals were used for cell transplantation [42]. Moreover, in contrast to those studies that mainly examined donor-derived microglia 2 months after transplantation, we characterized the donor-derived microglia up to 6 months post-transplant, which allowed the donor cells to develop for a longer term in the mouse brain. Although there were variations in chimerization among animals, this human microglia chimera model is highly reproducible according to scRNA-seq analysis using four chimeric mouse brains. We caculated the numbers of detected mouse/human microglia in each mouse brain sample and found that human microglia were consistently detected in each sample (legend to supplementary Figure 7). In addition, the high reproducibility of generating such a hiPSC microglial chimeric mouse brain model was also corroborated by two other recent reports [31, 93].

Remarkably, we find that xenografted hiPSC-derived microglia developed in the mouse brain retain a human microglial identity. Importantly, xenografted hiPSC-derived microglia showed expression patterns of microglial maturity resembling adult human microglia derived from human brain tissue. Therefore, establishment of such a hiPSC microglial chimeric mouse model provides novel opportunities for understanding the biology of human microglia. First, this proof-of-concept study paves the path to interrogating the species differences between human vs. mouse microglia at molecular, functional, and behavioral levels using this hiPSC microglia chimeric mouse brain model. It has been increasingly recognized that as compared to mouse microglia, human microglia possess unique features under conditions of development, aging and disease [8, 11-13]. In our model, human and mouse microglia develop in the same brain, but we have observed that human microglia are morphologically distinct from their mouse counterparts and also exhibit signature gene expression profiles characteristic of human microglia isolated from brain. Microglia are intimately involved in processes of neuronal development, such as neurogenesis, synaptogenesis, and synaptic pruning [94-96]. Building upon the

differential expression profiles, our model will be useful to investigate how human and mouse microglia function differently in shaping neuronal development. Similar to a recent report [31], our engrafted PMPs give to a small population of CNS macrophages. There are also potentially mouse-derived CNS macrophages in the brain tissue that we collected for single-cell RNA-seq, but likely to represent a small fraction of the total cluster. Therefore, within microglial clusters from each species, results may include some similar but distinguishable cell types. However, the primary gene expression differences are likely to be driven by the majority microglia. This was also supported by the observation that previously-reported signature genes expressed in human vs. mouse microglia [8] were differentially expressed in our results. Nevertheless, we take a conservative interpretation and did not claim to identify any novel gene expression differences between human vs. mouse microglia based on the current RNA-seq data. Second, a previous study reports that engrafted human astrocytes modulate other CNS cell types in the mouse brain, particularly enhancing neuronal synaptic plasticity [24]. Thus, in future studies, our hiPSC microglial chimeric mouse model will provide fascinating opportunities to understand how the inclusion of human microglia in the developing brain ultimately impacts neuronal development, synaptic plasticity, as well as the behavioral performance of the animals. Third, several transcriptomic studies [12, 20] have clearly demonstrated that microglial genes are differently regulated during aging and neurodegeneration between mice and humans, indicating the importance of developing a human microglia model to study human microglial function across different development stages, particularly adult microglia for studying aging-related and neurodegenerative disorders. our single-cell RNA-seq data suggests that Xeno MG resemble to adult human microglia. Moreover, functional analyses demonstrate that Xeno MG are dynamic in response to cuprizone-induced demyelination and recapitulate the upregulated expression of CD74 and SPP1 seen in MS patients[83], providing proof of concept that our chimeric mouse model has the ability to exhibit functional changes of human microglia under disease conditions. Combined with human iPSC technologies, such as the availability of edited, isogenic cells with or without disease-related genes, the hiPSC microglia chimeric mouse model will be informative in teasing out the roles of human microglia in neurodevelopmental disorders, neurodegenerative disorders, as well as brain infections by viruses such as Zika virus and HIV-1.

Similar to reports of hiPSC macroglial or neuronal chimeric mouse brain models [21, 24, 91], in the current hPSC microglial chimeric mouse model, the endogenous mouse counterpart cells are still present. In contrast to macroglial cells and neurons, microglial cells can be acutely depleted (up to 99% depletion) in the entire brain without significantly affecting the viability of animals, by pharmacologically inhibiting signaling pathways that are important for the survival and development of microglia, such as colony-stimulating factor 1 (CSF1) signaling [97] or by genetically coupling suicide genes under the control of promoters of microglia-specific genes [1, 98]. In future studies, it will be interesting to explore the possibility of creating humanized mouse brains containing solely hiPSC-derived microglia, by depleting endogenous mouse microglia using pharmacological or genetic approaches in neonatal mouse brains prior to engraftment of hiPSC-derived microglia. In addition, co-transplantation of human PSC-derived PMPs and neural or macroglial progenitors may generate chimeric mouse brain containing human microglia, neurons, and macroglial cells. Currently, in this proof-of-concept hPSC microglial chimeric mouse brain model, there is a lack of peripheral adaptive immune system in the host due to a *Rag2*$^{-/-}$ mutation. To circumvent this limitation, hiPSC-derived PMPs can be transplanted into animals in which the immune system is humanized by the same hiPSC-derived hematopoietic stem cells [36, 99, 100]. This will further allow the generation of animals with isogenic adaptive immune system and brain innate immune system derived from the same human individuals. Combined with recently developed hiPSC cerebral organoid models that contain microglia [16, 78], chimeric mouse brain models may help further our understanding of the complex interactions between human microglia and human neurons and macroglial cells under normal and disease conditions.

METHOD DETAILS

Generation, culture, and quality control of hPSC lines.

One healthy control female hiPSC line and female H9 ESC line were used this study. The hiPSC line were generated from healthy adult-derived fibroblasts using the "Yamanaka" reprogramming factors, as reported in our previous study [101] . The hiPSC line has been fully characterized by performing karyotyping, teratoma assay, DNA fingerprinting STR (short tandem repeat) analysis, gene expression profiling, and Pluritest (www.PluriTest.org), a robust open-access bioinformatic assay of pluripotency in human cells based on their gene expression profiles [102], as described in our previous study [101]. The hPSCs were maintained under feeder-free condition and cultured on dishes coated with hESC-qualified Matrigel (Corning) in mTeSR1 media (STEMCELL Technologies). Human PSCs from passage number 15 to 30 were used. The hPSCs were passaged approximately once per week with ReLeSR media (STEMCELL Technologies). All hPSC studies were approved by the Embryonic Stem Cell Research Oversight (ESCRO) committee at Rutgers University.

PMP generation and culture

PMP were generated from hiPSCs and H9 hESCs, using a published protocol [18]. Briefly, the yolk sac embryoid bodies (YS-EBs) were generated by treating the EBs with bone morphogenetic protein 4 (BMP4, 50 ng/ml, Peprotech; to induce mesoderm), vascular endothelial growth factor (VEGF, 50 ng/ml, Peprotech; endothelial precursors), and stem cell factor (SCF, 20 ng/ml, Miltenyi Biotech; hematopoietic precursors). Next, the YS-EBs were plated into dishes with interleukin-3 (IL-3, 25 ng/ml, Peprotech) and macrophage colony-stimulating factor (M-CSF, 100 ng/ml, Invitrogen) to promote myeloid differentiation. At 2–3 weeks after plating, human hPMPs emerged into the supernatant and were continuously produced for more than 3 months. The cumulative yield of PMPs was around 40-fold higher than the number of input hPSCs (Figure 1A), similar to the previous studies [16, 18]. PMPs were produced in a Myb-independent manner and closely recapitulating primitive hematopoiesis [118, 27].

Animals and Cell transplantation

PMP were collected from supernatant and suspended as single cells at a final concentration of 100,000 cells per µl in PBS. The cells were then injected into the brains of P0 Rag2$^{-/-}$hCSF1 immunodeficient mice (C;129S4-*Rag2*$^{tm1.1Flv}$ *Csf1tm1*$^{(CSF1)Flv}$ *Il2rg*$^{tm1.1Flv}$/J, The Jackson Laboratory). The precise transplantation sites were bilateral from the midline = ± 1.0 mm, posterior bregma = -2.0 mm, and dorsoventral depth = -1.5 and -1.2 mm (Figure 1C). The mouse pups were anesthetized by placing them on ice for 5 minutes. Once cryo-anesthetized, the pups were placed on a digital stereotaxic device (David KOPF Instruments), equipped with a neonatal mouse adaptor (Stoelting). The pups were then injected with 0.5 µl of cells into each site (total 4 sites) by directly inserting Hamilton needles through the skull into the target sites. The pups were weaned at 3 weeks and were kept up to 6 months before they were tested for the engraftment of human cells. All animal work was performed without gender bias with approval of the Institutional Animal Care and Use Committee (IACUC).

Both hiPSC- and hESC-derived PMPs were transplanted into mouse brains. Both engrafted hiPSC- and hESC-derived microglia were analyzed, including characterization of their marker expression (Figure 1), morphological changes along brain development (Figure 2), and their phagocytic functions under homeostatic condition (Figures 3), as well as toxin-induced demyelination condition (Figure 6). For the quantification, we pooled the data collected from both hiPSC- and hESC-derived microglia. In the single-cell RNA-sequencing experiment, we only used the animals received transplantation of hiPSC-derived microglia. For cuprizone-induced demyelination, three months old chimeric mice were fed with cuprizone diet (Sigma-Aldrich, 0.2%) or control diet for four weeks as previously report [103].

Sample preparation and library construction for Single-cell RNA sequencing

Six months old chimeric mice that received transplantation of microglia derived from the hiPSC line were used for single-cell RNA-sequencing experiments. The mice were perfused with oxygenated solution (2.5 mM KCl, 87 mM NaCl, 1.25 mM NaH_2PO_4, 26 mM $NaHCO_3$, 75 mM sucrose, 20 mM glucose, 2 mM $MgSO_4$, and1 mM $CaCl_2$) as reported [104] and the brain was quickly extracted and kept in the same cold solution for vibratome (VT1200, Leica) sectioning (500µm thickness) and dissection. The brain regions were isolated from where engrafted hiPSCs-derived microglia largely dispersed, including the cerebral cortex, hippocampus, corpus callosum, and olfactory bulb. The selected regions were chopped with Spring Scissors (WPI) into fine pieces for further dissociation into single cells, based on 10x Genomic Sample Preparation Domstratd Protocol (Dissociation of Mouse Embryonic Neural Tissue) with modifications. Briefly, the pieces were collected and dissociated with the Papain (1mg/ml, Sigma) and DNAase I (100 unit/ml, Roche) in Hibernate solution (Gibco) in 37℃ for 20 minutes. Tissues were washed and triturated with wide-bore tips in cold Hibernate solution until no visible chunks. The samples were spun down in 200 rcf for 2 minutes in 4℃ and filtered through 30 µm cell strainer to obtain single cells for cell counting and library preparation. To generate libraries, 20,000 cells were loaded for each sample. Chromium™ Single Cell 3' Library and Gel Bead Kit v2, 4 rxns, Chromium™ i7 Multiplex Kit, 96 rxns, and Chromium™ Single Cell A Chip Kit, 16 rxns are used from 10x Genomic single cell gene expression kit. cDNA libraries were generated following the manufacturer instructions.

Bulk and single-cell RNA sequencing

We performed bulk RNA-sequencing analysis of hiPSC-derived PMPs as previously reported [22]. Briefly, total RNA was prepared with RNAeasy kit (QIAGEN) and libraries were constructed using 600 ng of total RNA from each sample and the TruSeqV2 kit from Illumina (Illumina, San Diego, CA) following manufacturers suggested protocol. The libraries were subjected to 75 bp paired read sequencing using a NextSeq500 Illumina sequencer to generate approximately 30 to 36 million paired-reads per sample. Fastq files were generated using the Bc12Fastq software, version 1.8.4. The genome sequence was then indexed using the rsem-prepare-reference command. Each fastq file was trimmed using the fqtrim program, and then aligned to the human genome using the rsem-calculate-expression (version 1.2.31) command to calculate FPKM (fragments per kilobase of transcript per million mapped reads) values. In order to analyze the transcripts, FPKM > 1 was set as cutoff to filter transcripts.

For single-cell RNA sequencing, we have used Chromium™ i7 Multiplex Kit, 96 rxns, Chromium™ Single Cell 3' Library and Gel Bead Kit v2 and Chromium™ Single Cell A Chip Kit for capture and library preparation. Single cell RNA sequencing was performed by RUCDR® Infinite Biologics at Rutgers by using a 10X Genomics single cell gene expression profiling kit.The libraries were analyzed on Agilent 4200 TapeStation System using High Sensitivity D1000 ScreenTape Assay (Cat #: 5067-5584) and quantified using KAPA qPCR (Cat # KK4835). Libraries and then normalized to 10nM before being pooled together. The pooled library was then clustered and sequenced on Illumina HiSeq 2500 in Rapid Run Mode, using the following parameters: 36bp forward read, 100bp reverse read, and 8bp index read. For each individual library, the sequencing data from 4 unique indexes were combined before further analysis.

Sequencing reads were aligned with pooled mouse (mm10) and human (hg19) reference genomes and the barcodes were interpreted using Cellranger software (10X Genomics, v. 3.0.0). The resulting matrices of gene counts x barcodes were coded by individual sample identifier and loaded into Seurat (v. 3.0.0) software [105-107] in R/Bioconductor [108]. An initial analysis revealed a distinct cluster of human-expressing cells. To compare expression across species, a strategy was employed similar to one used previously [109]. A table of 17,629 unique matching genes was prepared, starting with a human-mouse gene homology list obtained from Jackson Labs (http://www.informatics.jax.org/downloads/reports/index.html#marker), and hand-curating to remove duplicates. The homologous genes list is deposited in a public data archive at https://github.com/rhart604/mousify/blob/master/geneTrans.txt. Sample/barcode identifiers for the human-specific data were isolated and matching gene symbols were converted from human to mouse.

Sample/barcode identifiers not matching this cluster were assumed to be mouse, and these were trimmed to retain only mouse gene symbols matching the homology list. Complete details of homology gene translation are described elsewhere [110].

To model both human and mouse results in a comparable system, we assigned individual sequencing reads to the optimal species using the alignment score in the bam file, and then separated the original fastq files into individual sets specific by species. These were re-processed with separated mouse or human reference genome indices and then recombined after translating homologous genes. In the end, only 147 out of 19,154 barcodes, or 0.76%, included sequences optimally aligning with both species, likely caused by the creation of droplets containing cells from more than one species, so these were eliminated from further consideration. The entire procedure, along with comparisons to alternative strategies, including all required R and Python code, is described elsewhere[110].

For analysis of human microglial sub-clusters, extracted human sample/barcode were restricted to human gene symbol results and re-analyzed with Seurat. Gene ontology analysis used the g:Profiler [111] website (https://biit.cs.ut.ee/gprofiler/gost).

For comparisons among sources of human microglia, raw RNAseq reads from the human-specific cluster were pooled by sample and aligned with reference human genome (hg38) using HISAT2 [112]. Raw sequencing reads from other publications were downloaded from GEO (series accessions GSE99074[12], GSE97744[17], GSE102335[78], and GSE133434[42]). After similar HISAT2 alignment, all count summaries were imported into a DESeq2 [113] data model and a variance stabilization transformation was applied prior to principal components analysis.

Immunostaining and cell counting

Mouse brains fixed with 4% paraformaldehyde were put in 20% and 30% sucrose for dehydration. After dehydration, brain tissues were blocked with OCT and frozen by solution of dry ice and pure alcohol. The frozen tissues were cryo-sectioned with 30 μm thickness for immunofluorescence staining [114, 115]. The tissues were blocked with blocking solution (5% goat or donkey serum in PBS with Triton X-100) in room temperature (RT) for 1 hr. The Triton X-100 concentration was 0.8% for brain tissue. The primary antibodies were diluted in the same blocking solution and incubated with tissues in 4 °C overnight. The primary antibodies were listed in supplementary Table S3. Then, the sections were washed with PBS and incubated with secondary antibodies for 1 hr in RT. After washing with PBS, the slides were mounted with the anti-fade Fluoromount-G medium containing 1, 40,6-diamidino-2-phenylindole dihydrochloride (DAPI) (Southern Biotechnology). For PSD95 peptide blocking experiment, PSD95 antibody (2.5 μg/ml) was incubated with five times PSD95 blocking peptide (12.5 μg/ml, Synaptic System) or equivalent amount of PBS at RT for 30 minutes before applying secondary antibodies to the brain tissues as suggested by the manufacturer instructions.

Images were captured with a Zeiss 710 confocal microscope. Large scale images in Figure 1D, supplementary Figure 1A and 1B were obtained by confocal tile scan and automatically stitched using 10% overlap between tiles by Zen software (Zeiss). For 3D reconstructive images in Figure 3E, Figure 6A and Supplementary Figure 6B, 6D and 6E were processed by Zen software (Zeiss). To visualize synaptic puncta pruning, myelin debris engulfment, super-resolution images in Figure 3A, 3B, 3D, Figure 6B, 4C, Supplementary Figure 5 and Supplementary Figure 6A, 6C were acquired by Zeiss Airyscan super-resolution microscope at 63X with 0.2 mm z-steps. Cell number and microglia process length and endpoints were counted with ImageJ software, following our previous report [22]and the published protocol [116]. At least five consecutive sections of each brain region were chosen. The number of positive cells from each section was counted after a Z projection and at least 7 mice in each group were counted. The number of synaptic puncta or myelin debris were calculated from 7 mice in each group, minimal 10 cells per animal. Engraftment efficiency and degree of chimerization were assessed by quantifying the percentage of $hTMEM119^+$ cells among total $DAPI^+$ cells in sagittal brain sections, as reported in the previous studies [24, 25]. The cell counting was performed on every fifteenth sagittal brain section with a distance of 300 μm, covering brain regions from 0.3 to 2.4 mm lateral to the midline (seven to eight sections from each mouse brain were used).

Data analysis

All data represent mean ± s.e.m. For the data presented as bar-and-data overlap plots. When only two independent groups were compared, significance was determined by two-tailed unpaired t-test with Welch's correction. When three or more groups were compared, one-way ANOVA with Bonferroni post hoc test or two-way ANOVA was used. A P value less than 0.05 was considered significant. The analyses were done in GraphPad Prism v.5.

Data availability

The accession number of the single-cell RNA sequencing data reported in this study is GEO: GSE129178.

Acknowledgements

This work was in part supported by grants from the NIH (R21HD091512 and R01NS102382 to P.J.) R.P.H. was supported by R01ES026057, R01AA023797, and U10AA008401. X.L. was supported by the Jiangsu Government Scholarship for Overseas Studies from China. We thank Dr. Cheryl Dreyfus from Rutgers Robert Wood Johnson Medical School for the suggestions on cuprizone model, Dr. Noriko Kane-Goldsmith from Rutgers University for assistance with Zeiss Airyscan super-resolution imaging, and Dr. Brian Daniels from Rutgers University for critical reading of the manuscript. We also thank Ms. Maharaib Syed from Rutgers University for the assistance with immunohistochemistry.

Author Contributions

P.J. and R.X. designed experiments and interpreted data; R.X. carried out most of experiments with technical assistance from A.B., X.L., A.P., and K.K.; R.P.H. performed the gene expression analysis, interpreted the data, and provided critical suggestions to the overall research direction; P.J. directed the project and wrote the manuscript together with R.X. and input from all co-authors.

Competing Financial Interests

The authors declare no competing financial interests.

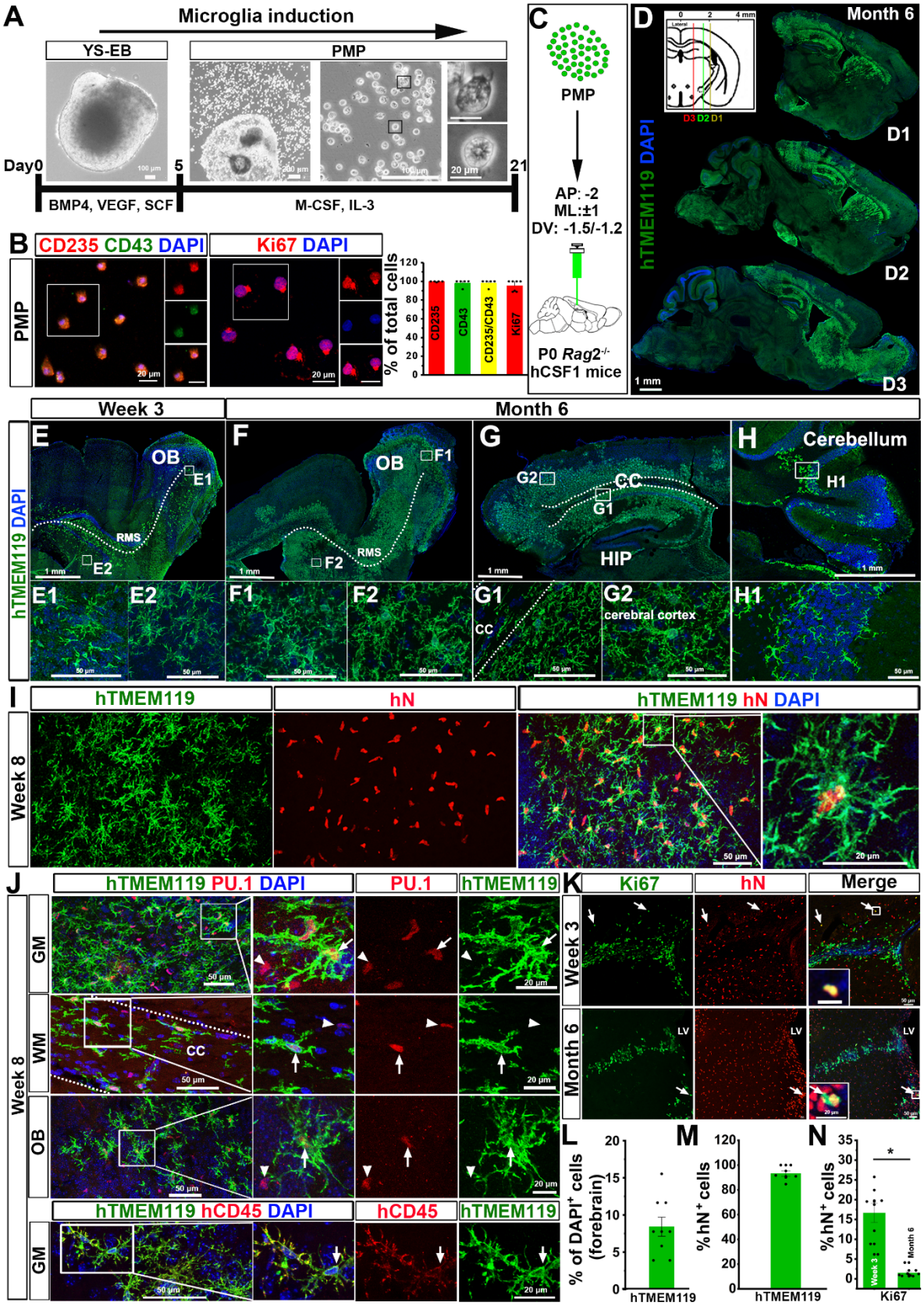
A
Microglia induction
YS-EB
PMP
Day0
5
21
BMP4, VEGF, SCF
M-CSF, IL-3
B
CD235 CD43 DAPI
Ki67 DAPI
PMP
% of total cells
CD235
CD43
CD235/CD43
Ki67
C
PMP
AP: -2
ML:±1
DV: -1.5/-1.2
P0 Rag2-/-
hCSF1 mice
D
Month 6
hTMEM119 DAPI
D1
D2
D3
Week 3
Month 6
E
F
G
H
OB
RMS
HIP
CC
Cerebellum
cerebral cortex
I
hTMEM119
hN
hTMEM119 hN DAPI
Week 8
J
hTMEM119 PU.1 DAPI
PU.1
hTMEM119
GM
WM
OB
hTMEM119 hCD45 DAPI
hCD45
K
Ki67
hN
Merge
Week 3
Month 6
LV
L
% of DAPI+ cells (forebrain)
M
% hN+ cells
N
% hN+ cells
Week 3
Month 6
Ki67

1

Figure 1. Generation of hPSC microglial chimeric mouse brains.

(A) A schematic procedure for generating primitive macrophage precursor (PMP) from hiPSCs or hESCs-derived yolk sac embryoid bodies (YS-EB). Insets: representative bright-field images at different stages. Scale bars represent 100 μm, 200 μm, and 20 μm as indicated in the images

(B) Representative images and quantification of $CD235^+$, $CD43^+$, $CD235^+/CD43^+$, and $Ki67^+$ cells in PMP. Quantification of pooled data from one hiPSC line and one hESC line. The experiments are repeated for at least 5 times (n = 5-7) and for each experiment, the two stem cell lines are used. Data are presented as mean ± s.e.m. Scale bars: 20 μm in the original and enlarged images.

(C) A schematic diagram showing that hPSC-derived PMP are engrafted into the brains of P0 *rag*$2^{-/-}$ hCSF1 mice.

(D) Representative images from sagittal brain sections showing the wide distribution of xenografted hPSC-derived microglia at six months post-transplantation. Anti-human-specific TMEM119 (hTMEM119) selectively labels xenografted hPSC-derived microglia. Scale bar: 1 mm.

(E-H) Representative images from sagittal brain sections showing the distribution of $hTMEM119^+$ xenografted hPSC-derived microglia at 3 weeks and 6 months post-transplantation in different brain regions. OB, olfactory bulb; RMS, rostral migratory stream; CC, corpus callosum; HIP, Hippocampus. Scale bars: 1 mm or 50 μm in the original or enlarged images, respectively.

(I) Representative images of $hTMEM119^+$ cells among the total donor-derived hN^+ cells in grey matter at 8 weeks post-transplantation. Scale bars, 50 μm or 20 μm in the original or enlarged images, respectively.

(J) Representative images of PU.1- and human-specific CD45 (hCD45)-expressing cells in the donor-derived $hTMEM119^+$ cells in different brain regions at 8 weeks post-transplantation. Scale bars, 50 μm or 20 μm in the original or enlarged images, respectively.

(K) Representative images of $Ki67^+$ cells among the total donor-derived hN^+ cells at 3 weeks and 6 months post-transplantation. Scale bars, 50 μm or 20 μm in the original or enlarged images, respectively.

(L) Quantification of the percentage of $hTMEM119^+$ cells in total $DAPI^+$ cells in the forebrain at 6 months post-transplantation (n = 9 mice). The data are pooled from the mice received transplantation of microglia derived from both hESCs and hiPSCs. Data are presented as mean ± s.e.m.

(M) Quantification of the percentage of $hTMEM119^+$ cells in total hN^+ cells (n = 7 mice). Data are presented as mean ± s.e.m.

(N) Quantification of $Ki67^+$ cells among the total donor-derived hN^+ cells at 3 weeks or 6 months post-transplantation (n = 8 mice for each time point). The data are pooled from the mice that received transplantation of microglia derived from both hESCs and hiPSCs. Student's *t* test. $^{**}P < 0.01$. Data are presented as mean ± s.e.m.

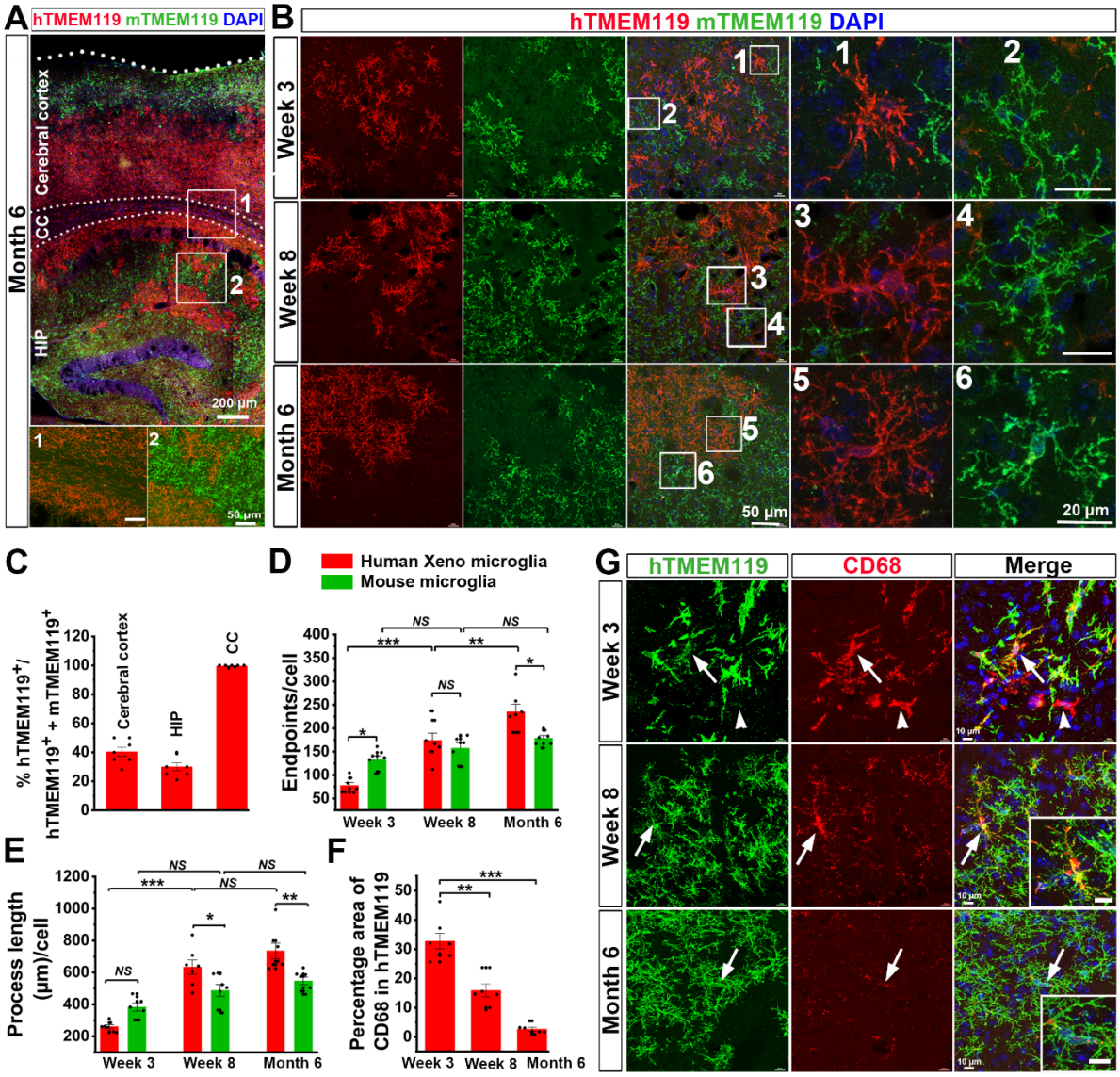
A
hTMEM119 mTMEM119 DAPI
Month 6
Cerebral cortex
CC
HIP
200 µm
50 µm
B
hTMEM119 mTMEM119 DAPI
Week 3
Week 8
Month 6
50 µm
20 µm
C
% hTMEM119+/ hTMEM119+ + mTMEM119+
Cerebral cortex
HIP
CC
D
Human Xeno microglia
Mouse microglia
Endpoints/cell
Week 3
Week 8
Month 6
E
Process length (µm)/cell
F
Percentage area of CD68 in hTMEM119
G
hTMEM119
CD68
Merge
Week 3
Week 8
Month 6

1

Figure 2. Human PSC-derived microglia undergo morphological maturation.

(A) Representative images of hTMEM119$^+$ hPSC-derived microglia and mTMEM119$^+$ mouse microglia in the cerebral cortex, corpus callosum (CC) and hippocampus (HIP) in 6 months old mice. Scale bars represent 200 μm and 50 μm in the original and enlarged images, respectively.

(B) Representative images of hTMEM119$^+$ hPSC-derived microglia and mTMEM119$^+$ mouse microglia in the cerebral cortex in 3 weeks, 8 weeks, and 6 months old mice. Scale bars represent 50 μm and 20 μm in the original and enlarged images, respectively.

(C) Quantification of the percentage of hTMEM119$^+$ cells in total microglia (hTMEM119$^+$ plus mTMEM119$^+$) in the cerebral cortex, hippocampus (HIP), corpus callosum (CC) in 6 months old chimeric mice (n = 7 mice for each time point). The data are pooled from the mice received transplantation of microglia derived from both hESCs and hiPSCs. Data are presented as mean ± s.e.m.

(D and E) Quantification of endpoint numbers and total process length of mouse and hPSC-derived microglia based on mTMEM119 or hTMEM119 staining respectively from grey matter at the three time points (n = 7 mice for each time point). The data are pooled from the mice received transplantation of microglia derived from both hESCs and hiPSCs. Two-way ANOVA is used to compare the endpoints and process length between human and mouse microglia and one-way ANOVA is used for the comparison within mouse or human microglia. *P < 0.05, ***P < 0.001, NS, no significance. Data are presented as mean ± s.e.m.

(F) Quantification of the percentage of CD68$^+$ area in hTMEM119$^+$ area from cerebral cortex in 3 weeks, 8 weeks and 6 months old chimeric mice (n = 7 mice for each time point). The data are pooled from the mice received transplantation of microglia derived from both hESCs and hiPSCs. One-way ANOVA test, **P < 0.01, ***P < 0.001. Data are presented as mean ± s.e.m.

(G) Representative images of CD68- and hTMEM119-exprssing cells in the cerebral cortex from 3 weeks, 8 weeks and 6 months old mice. Scale bars, 10 μm or 2 μm in the original or enlarged images, respectively.

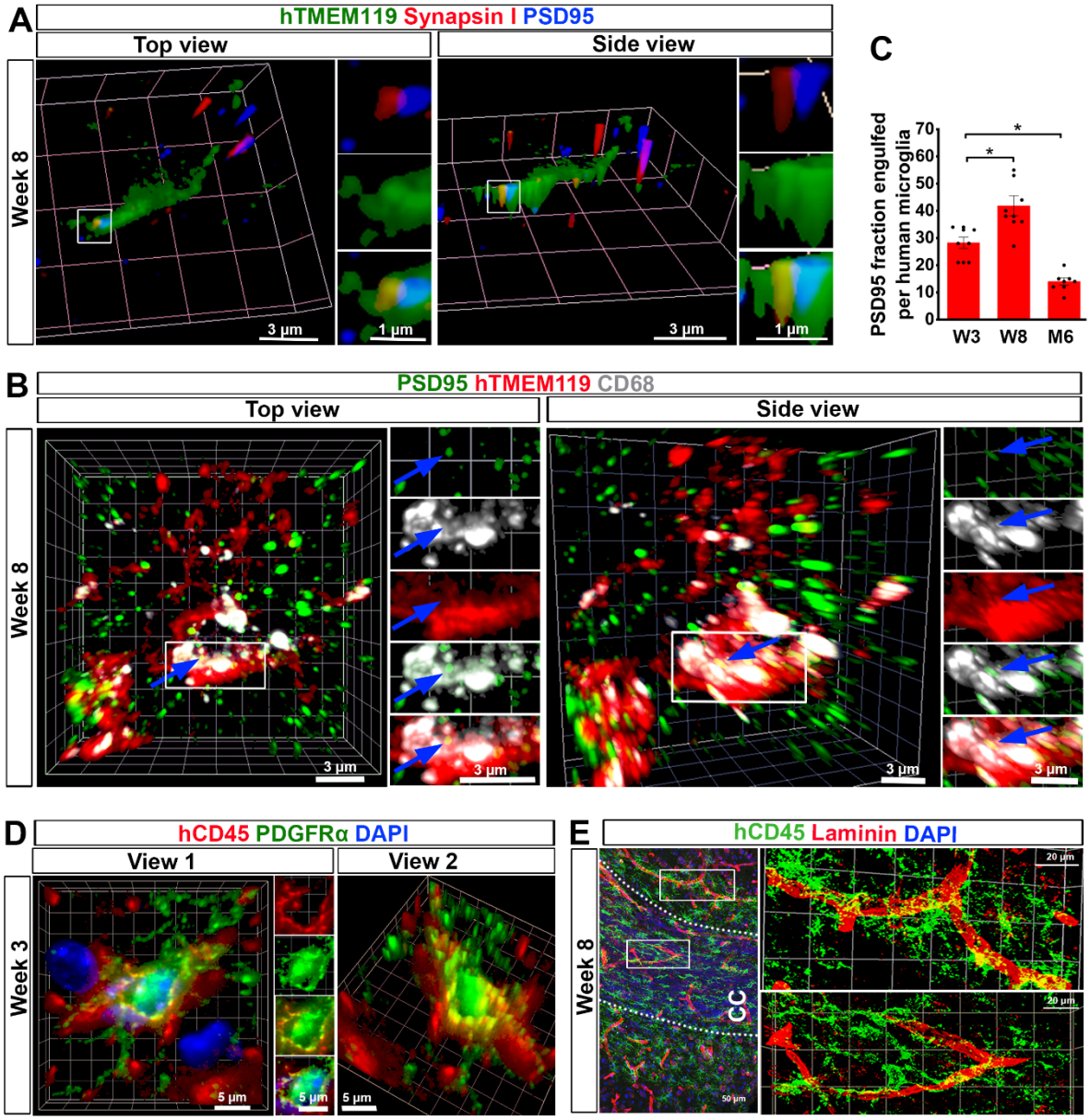
A
hTMEM119 Synapsin I PSD95
Top view
Side view
Week 8
3 µm
1 µm
C
PSD95 fraction engulfed per human microglia
70
60
50
40
30
20
10
0
W3
W8
M6
B
PSD95 hTMEM119 CD68
Top view
Side view
Week 8
3 µm
D
hCD45 PDGFRα DAPI
View 1
View 2
Week 3
5 µm
E
hCD45 Laminin DAPI
Week 8
CC
20 µm
50 µm

1

Figure 3. Human PSC-derived microglia are functional in the mouse brain.
(A) Representative 3D reconstruction of super-resolution images showing hTMEM119$^+$ donor-derived microglia engulf synaptic proteins, synapsin I and PSD95 in grey matter at 8 weeks post-transplantation. Scale bars, 3 and 1μm in the original or enlarged images, respectively.
(B) Representative 3D reconstruction of super-resolution images showing colocalization of hTMEM119, PSD95, and CD68 staining in grey matter at 8 weeks post-transplantation. Scale bars, 3 in the original and enlarged images.
(C) Quantification of PSD95$^+$ fraction engulfed per microglia from cerebral cortex at the three time points (n = 7 mice for each time point). The data are pooled from the mice received transplantation of microglia derived from both hESCs and hiPSCs One-way ANOVA test, *$P < 0.05$. Data are presented as mean ± s.e.m.
(D) Representative 3D reconstruction of super-resolution images showing that hCD45$^+$ hPSC-derived microglia phagocytize PDGFRα$^+$ oligodendroglial cells in the corpus callosum at 3 weeks post-transplantation. Scale bars, 5 μm.
(E) Representative images showing the interaction between laminin$^+$ blood vessels and hCD45$^+$ human microglia in grey matter and white matter at 8 weeks post-transplantation. Scale bars, 50 and 20 μm in the original or enlarged images, respectively.

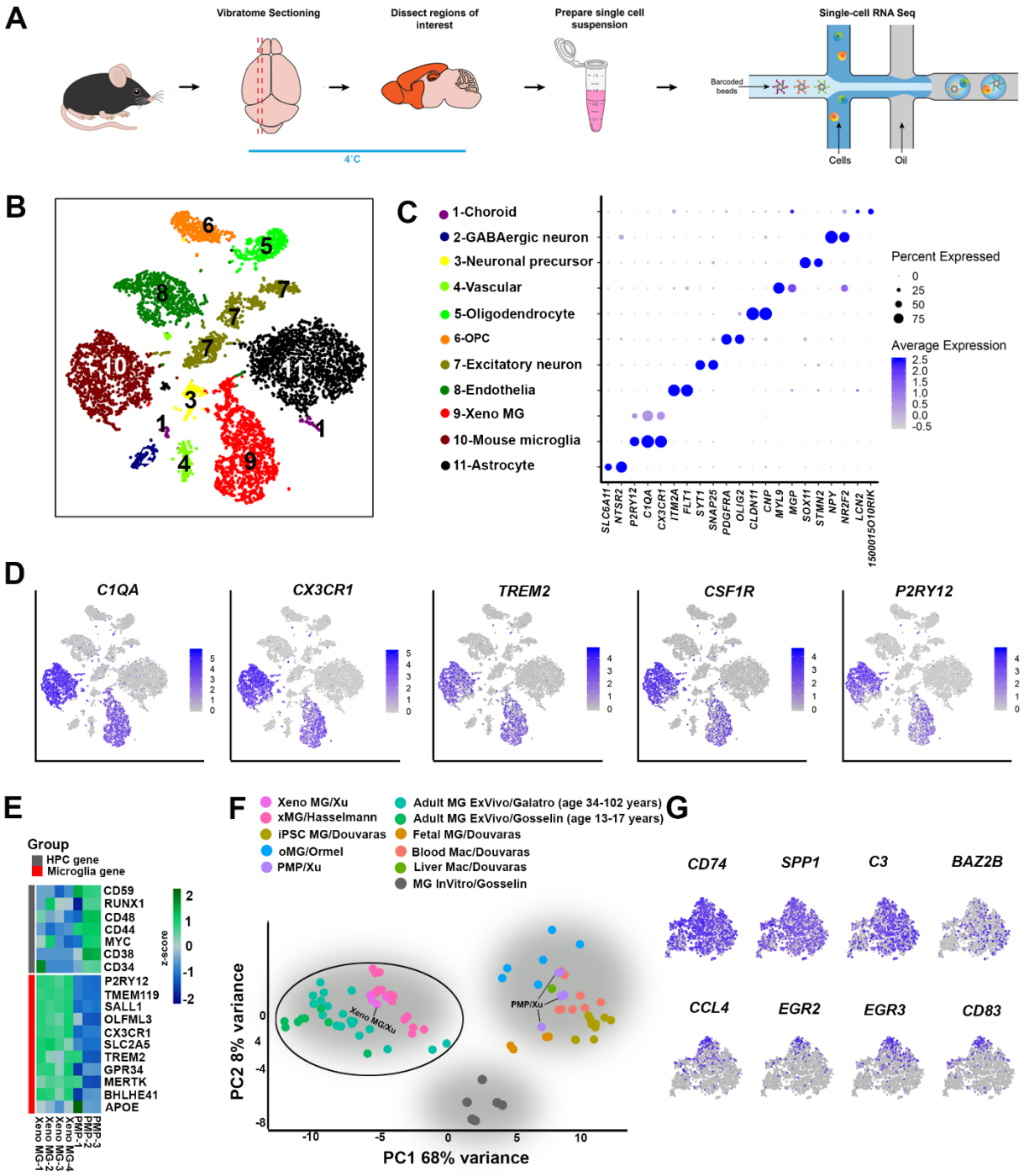
A
Vibratome Sectioning
Dissect regions of interest
Prepare single cell suspension
Single-cell RNA Seq
Barcoded beads
Cells
Oil
4°C
B
C
1-Choroid
2-GABAergic neuron
3-Neuronal precursor
4-Vascular
5-Oligodendrocyte
6-OPC
7-Excitatory neuron
8-Endothelia
9-Xeno MG
10-Mouse microglia
11-Astrocyte
Percent Expressed
Average Expression
SLC6A11
NTSR2
P2RY12
C1QA
CX3CR1
ITM2A
FLT1
SYT1
SNAP25
PDGFRA
OLIG2
CLDN11
CNP
MYL9
MGP
SOX11
STMN2
NPY
NR2F2
LCN2
1500015O10RIK
D
C1QA
CX3CR1
TREM2
CSF1R
P2RY12
E
Group
HPC gene
Microglia gene
CD59
RUNX1
CD48
CD44
MYC
CD38
CD34
P2RY12
TMEM119
SALL1
OLFML3
CX3CR1
SLC2A5
TREM2
GPR34
MERTK
BHLHE41
APOE
z-score
Xeno MG-1
Xeno MG-2
Xeno MG-3
Xeno MG-4
PMP-1
PMP-2
PMP-3
F
Xeno MG/Xu
xMG/Hasselmann
iPSC MG/Douvaras
oMG/Ormel
PMP/Xu
Adult MG ExVivo/Galatro (age 34-102 years)
Adult MG ExVivo/Gosselin (age 13-17 years)
Fetal MG/Douvaras
Blood Mac/Douvaras
Liver Mac/Douvaras
MG InVitro/Gosselin
PC2 8% variance
PC1 68% variance
G
CD74
SPP1
C3
BAZ2B
CCL4
EGR2
EGR3
CD83

Figure 4. Single-cell RNA-seq analysis of hiPSC microglial chimeric mouse brain.
(A) A schematic diagram showing the experimental design. Microglia were isolated from the highlighted brain regions at 6 months post-transplantation and handled at 4°C to reduce ex vivo activation. The single-cell suspension was loaded into a 10X Genomics Chromium system for single-cell RNA-sequencing.
(B) tSNE plot of 11 cell types as identified by characteristic cell-specific gene expression, following translation of human gene symbols to mouse symbols as described in Methods. Arrow indicates the human xenograft microglia (Xeno MG).
(C) Dot plot showing two representative cell-specific genes for each cell cluster. As indicated by the legend, the diameter of the dot indicates the percent of cells within a cluster expressing the gene (percent expression). The color saturation indicates the average expression over the cluster (average expression; log normalized counts). The cluster numbers, colors of clusters in panel B, and selected cell identities are shown at left.
(D) tSNE plots with dots (representing individual barcodes/cells) colored by expression of canonical microglial genes, based on expression level determined in Seurat (log normalized counts).
(E) A heatmap showing expression of signature genes of hematopoietic progenitor cells (HPC) and microglia in PMPs and Xeno MG, showing individual replicates (n=3 for PMP, n=4 averaged human clusters for Xeno MG). Color indicates the expression level normalized for each gene using a Z-score.
(F) Principal component analysis (PCA) of our Xeno MG, hiPSC-derived PMPs, and individual cell RNA-seq expression data from publicly-available datasets, including hiPSC-derived microglia cultured under 2-dimensional (2D) conditions (iPS MG)[17, 77], hiPSC-derived microglia developed in 3D cerebral organoids (oMG)[78], hiPSC-derived microglia developed for 2-7.8 months in mouse brain (xMG) [42]. brain-tissue derived adult human microglia, including adult ex vivo microglia (Adult MG ExVivo) from Gosselin et al., 2017[8] (age from 13-17 years) and Galatro et al., 2017 (age from 34-102 years) [12], in vitro microglia (MG InVitro) from Gosselin et al., 2017[8], as well as blood/liver macrophages [17, 77].
(G) t-SNE plots of selected human cells showing the expression of *CD74, SPP1, C3, BAZ2B, CCL4, EGR2, EGR3,* and *CD83* gene transcripts. *CD74*, *SPP1*, *C3* and *BAZ2B* appear to be uniformly expressed in all cells, but *CCL4, EGR2, EGR3,* and *CD83* are enriched in distinct subsets of in Xeno MG.

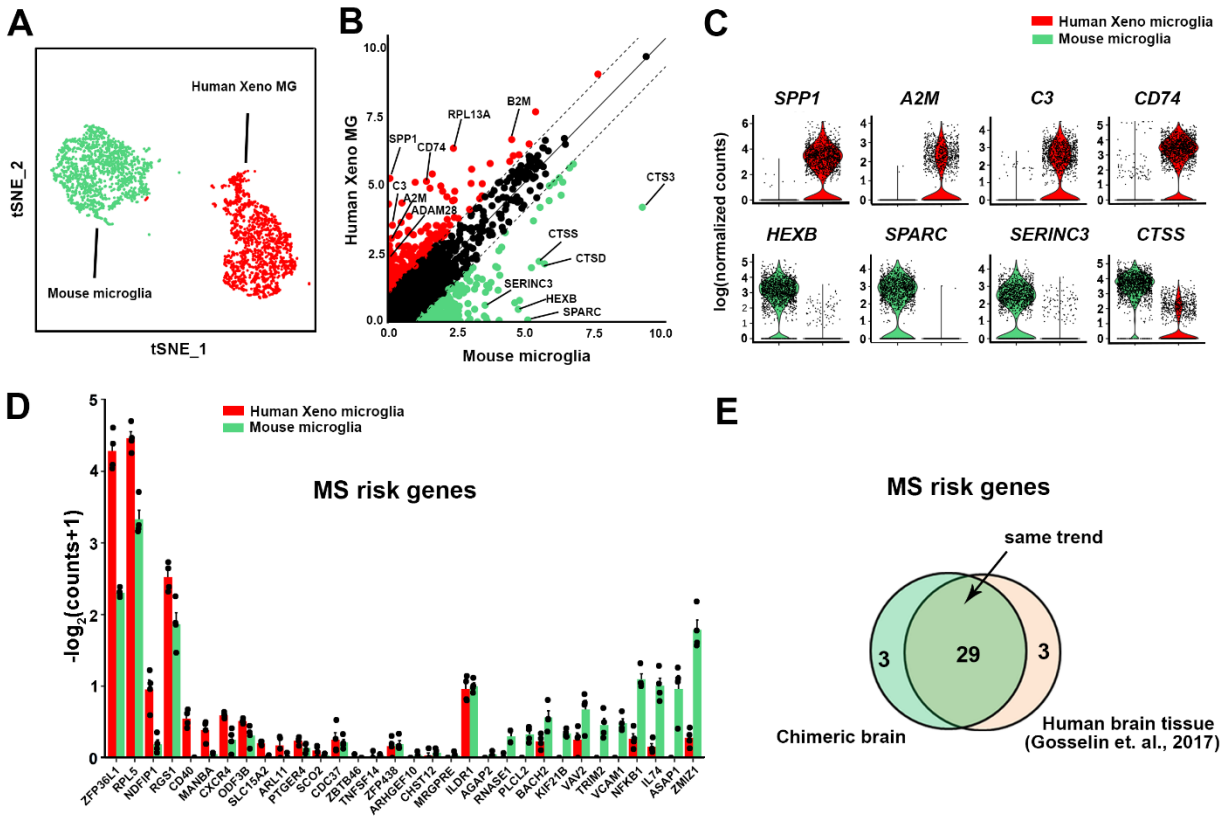
A
Human Xeno MG
Mouse microglia
tSNE_2
tSNE_1
B
Human Xeno MG
Mouse microglia
SPP1
CD74
C3
A2M
ADAM28
RPL13A
B2M
CTS3
CTSS
CTSD
SERINC3
HEXB
SPARC
C
Human Xeno microglia
Mouse microglia
SPP1
A2M
C3
CD74
HEXB
SPARC
SERINC3
CTSS
log(normalized counts)
D
Human Xeno microglia
Mouse microglia
MS risk genes
-log2(counts+1)
ZFP36L1
RPL5
NDFIP1
RGS1
CD40
MANBA
CXCR4
ODF3B
SLC15A2
ARL11
PTGER4
SCCO2
CDC37
ZBTB46
TNFSF14
ZFP438
ARHGEF10
CHST12
MRGPRE
ILDR1
AGAP2
RNASE1
PLCL2
BACH2
KIF21B
VAV2
TRIM2
VCAM1
NFKB1
IL7A
ASAP1
ZMIZ1
E
MS risk genes
same trend
3
29
3
Chimeric brain
Human brain tissue
(Gosselin et. al., 2017)

Figure 5. Transcriptomic profiling analysis of clusters of Xeno MG and mouse microglia.
(A) tSNE plot highlighting only the clusters of human Xeno MG and mouse host microglia.
(B) Scatter plot showing mean mRNA expression levels of human and mouse genes with unique orthologs from Xeno MG and mouse microglia clusters, highlighting the differentially expressed genes (DEGs; at least two-fold different) in human Xeno MG (red) or mouse microglia (green) from 6 months old chimeric mouse brain. Significantly different DEGs (less than 5% false discovery rate [FDR] and at least two-fold different) are listed in Table S2.
(C) Violin plots summarizing expression differences in individual cells within the human Xeno MG and mouse microglia clusters. Dots indicate expression levels (as log normalized counts) of individual cells and the violin shape summarizes the distribution of expression in the population.
(D) Bar plots showing the average expression (mean ± SEM, n = 4 samples) of Multiple sclerosis (MS)-associated genes in Xeno MG and mouse microglia. These genes were reported to be differentially expressed between human and mouse microglia as in Gosselin et al., 2017 [8].
(E) Venn diagrams showing that majority of the MS associated genes that were reported to be differentially expressed between human and mouse microglia are recapitulated in our chimeric mouse model (29 of 32).

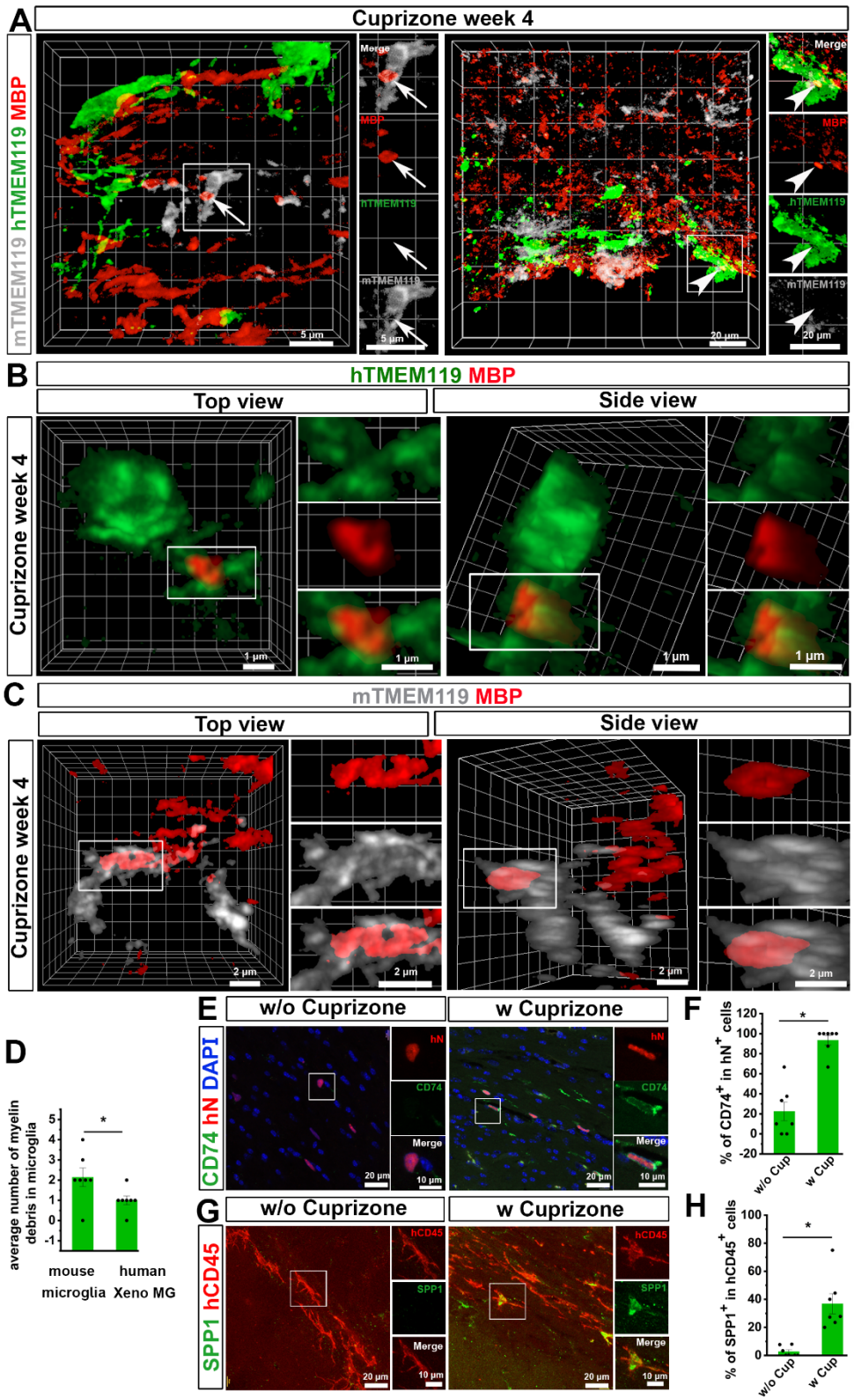
A
Cuprizone week 4
mTMEM119 hTMEM119 MBP
Merge
MBP
hTMEM119
mTMEM119
5 µm
20 µm
B
hTMEM119 MBP
Top view
Side view
Cuprizone week 4
1 µm
C
mTMEM119 MBP
Top view
Side view
Cuprizone week 4
2 µm
D
average number of myelin debris in microglia
mouse microglia
human Xeno MG
E
w/o Cuprizone
w Cuprizone
CD74 hN DAPI
hN
CD74
Merge
20 µm
10 µm
F
% of CD74+ in hN+ cells
w/o Cup
w Cup
G
w/o Cuprizone
w Cuprizone
SPP1 hCD45
hCD45
SPP1
Merge
H
% of SPP1+ in hCD45+ cells
w/o Cup
w Cup

Figure 6. Responses of hPSC-derived microglia to cuprizone-induced demyelination.
(A) Representative 3D reconstruction images showing hTMEM119$^+$ donor-derived microglia and mTMEM119$^+$ mouse host microglia interact with MBP$^+$ myelin debris in the corpus callosum after 4 weeks of cuprizone-diet. Scale bars, 5 or 20 μm in the original or enlarged images as indicated.
(B and C) Representative 3D reconstruction of super-resolution images showing hTMEM119$^+$ donor-derived microglia (B) and mTMEM119$^+$ mouse host microglia (C) engulf MBP$^+$ myelin debris in the corpus callosum after 4 weeks of cuprizone-diet. Scale bars, 1 μm in the original or enlarged images.
(D) Quantification of average number of myelin debris in mouse host microglia and human Xeno MG (n = 7 mice). The data are pooled from the mice that received transplantation of microglia derived from both hESCs and hiPSCs. Student's *t* test. $^*P < 0.05$. Data are presented as mean ± s.e.m.
(E) Representative images showing CD74$^+$ and hN$^+$ cells after 4 weeks of diet with (w) or without (w/o) cuprizone. Scale bars, 20 and 10 μm in the original or enlarged images, respectively.
(F) Quantification of the percentage of CD74$^+$ cells in total hN$^+$ cells after 4 weeks of diet with (w) or without (w/o) cuprizone (n = 7 mice). The data are pooled from the mice that received transplantation of microglia derived from both hESCs and hiPSCs. Student's *t* test. $^*P < 0.05$. Data are presented as mean ± s.e.m.
(G) Representative images showing SPP1$^+$ and hN$^+$ cells after 4 weeks of diet with (w) or without (w/o) cuprizone. Scale bars, 20 and 10 μm in the original or enlarged images, respectively.
(F) Quantification of the percentage of SPP1$^+$ cells in total hN$^+$ cells after 4 weeks of diet with (w) or without (w/o) cuprizone (n = 7 mice). The data are pooled from the mice that received transplantation of microglia derived from both hESCs and hiPSCs. Student's *t* test. $^*P < 0.05$. Data are presented as mean ± s.e.m.

References:

1. Li, Q. & Barres, B.A. Microglia and macrophages in brain homeostasis and disease. *Nat Rev Immunol* **18**, 225-242 (2018).
2. Casano, A.M. & Peri, F. Microglia: multitasking specialists of the brain. *Dev Cell* **32**, 469-477 (2015).
3. Keren-Shaul, H. et al. A Unique Microglia Type Associated with Restricting Development of Alzheimer's Disease. *Cell* **169**, 1276-1290 e1217 (2017).
4. Hong, S. et al. Complement and microglia mediate early synapse loss in Alzheimer mouse models. *Science* **352**, 712-716 (2016).
5. Yeh, F.L., Wang, Y., Tom, I., Gonzalez, L.C. & Sheng, M. TREM2 Binds to Apolipoproteins, Including APOE and CLU/APOJ, and Thereby Facilitates Uptake of Amyloid-Beta by Microglia. *Neuron* **91**, 328-340 (2016).
6. Venegas, C. et al. Microglia-derived ASC specks cross-seed amyloid-beta in Alzheimer's disease. *Nature* **552**, 355-361 (2017).
7. Fuhrmann, M. et al. Microglial Cx3cr1 knockout prevents neuron loss in a mouse model of Alzheimer's disease. *Nat Neurosci* **13**, 411-413 (2010).
8. Gosselin, D. et al. An environment-dependent transcriptional network specifies human microglia identity. *Science* **356** (2017).
9. Hansen, D.V., Hanson, J.E. & Sheng, M. Microglia in Alzheimer's disease. *The Journal of cell biology* **217**, 459-472 (2018).
10. Holtman, I.R., Skola, D. & Glass, C.K. Transcriptional control of microglia phenotypes in health and disease. *J Clin Invest* **127**, 3220-3229 (2017).
11. Smith, A.M. & Dragunow, M. The human side of microglia. *Trends Neurosci* **37**, 125-135 (2014).
12. Galatro, T.F. et al. Transcriptomic analysis of purified human cortical microglia reveals age-associated changes. *Nat Neurosci* **20**, 1162-1171 (2017).
13. Friedman, B.A. et al. Diverse Brain Myeloid Expression Profiles Reveal Distinct Microglial Activation States and Aspects of Alzheimer's Disease Not Evident in Mouse Models. *Cell Rep* **22**, 832-847 (2018).
14. Muffat, J. et al. Efficient derivation of microglia-like cells from human pluripotent stem cells. *Nat Med* **22**, 1358-1367 (2016).
15. Pandya, H. et al. Differentiation of human and murine induced pluripotent stem cells to microglia-like cells. *Nat Neurosci* **20**, 753-759 (2017).
16. Abud, E.M. et al. iPSC-Derived Human Microglia-like Cells to Study Neurological Diseases. *Neuron* **94**, 278-293 e279 (2017).
17. Douvaras, P. et al. Directed Differentiation of Human Pluripotent Stem Cells to Microglia. *Stem Cell Reports* **8**, 1516-1524 (2017).
18. Haenseler, W. et al. A Highly Efficient Human Pluripotent Stem Cell Microglia Model Displays a Neuronal-Co-culture-Specific Expression Profile and Inflammatory Response. *Stem Cell Reports* **8**, 1727-1742 (2017).
19. Brownjohn, P.W. et al. Functional Studies of Missense TREM2 Mutations in Human Stem Cell-Derived Microglia. *Stem Cell Reports* **10**, 1294-1307 (2018).
20. Olah, M. et al. A transcriptomic atlas of aged human microglia. *Nat Commun* **9**, 539 (2018).
21. Chen, C., Kim, W.Y. & Jiang, P. Humanized neuronal chimeric mouse brain generated by neonatally engrafted human iPSC-derived primitive neural progenitor cells. *JCI Insight* **1**, e88632 (2016).

22. Xu, R. et al. OLIG2 Drives Abnormal Neurodevelopmental Phenotypes in Human iPSC-Based Organoid and Chimeric Mouse Models of Down Syndrome. *Cell Stem Cell* **24**, 908-926 e908 (2019).
23. Windrem, M.S. et al. Human iPSC Glial Mouse Chimeras Reveal Glial Contributions to Schizophrenia. *Cell Stem Cell* **21**, 195-208 e196 (2017).
24. Han, X. et al. Forebrain engraftment by human glial progenitor cells enhances synaptic plasticity and learning in adult mice. *Cell Stem Cell* **12**, 342-353 (2013).
25. Chen, H. et al. Human-derived neural progenitors functionally replace astrocytes in adult mice. *J Clin Invest* **125**, 1033-1042 (2015).
26. van Wilgenburg, B., Browne, C., Vowles, J. & Cowley, S.A. Efficient, long term production of monocyte-derived macrophages from human pluripotent stem cells under partly-defined and fully-defined conditions. *PLoS One* **8**, e71098 (2013).
27. Buchrieser, J., James, W. & Moore, M.D. Human Induced Pluripotent Stem Cell-Derived Macrophages Share Ontogeny with MYB-Independent Tissue-Resident Macrophages. *Stem Cell Reports* **8**, 334-345 (2017).
28. Claes, C., Van den Daele, J. & Verfaillie, C.M. Generating tissue-resident macrophages from pluripotent stem cells: Lessons learned from microglia. *Cell Immunol* **330**, 60-67 (2018).
29. Sturgeon, C.M., Ditadi, A., Awong, G., Kennedy, M. & Keller, G. Wnt signaling controls the specification of definitive and primitive hematopoiesis from human pluripotent stem cells. *Nat Biotechnol* **32**, 554-561 (2014).
30. Rathinam, C. et al. Efficient differentiation and function of human macrophages in humanized CSF-1 mice. *Blood* **118**, 3119-3128 (2011).
31. Hasselmann, J. et al. Development of a Chimeric Model to Study and Manipulate Human Microglia In Vivo. *Neuron* (2019).
32. Bennett, M.L. et al. New tools for studying microglia in the mouse and human CNS. *Proc Natl Acad Sci U S A* **113**, E1738-1746 (2016).
33. Forrester, J.V., McMenamin, P.G. & Dando, S.J. CNS infection and immune privilege. *Nat Rev Neurosci* **19**, 655-671 (2018).
34. Kettenmann, H., Hanisch, U.K., Noda, M. & Verkhratsky, A. Physiology of microglia. *Physiol Rev* **91**, 461-553 (2011).
35. McKercher, S.R. et al. Targeted disruption of the PU.1 gene results in multiple hematopoietic abnormalities. *EMBO J* **15**, 5647-5658 (1996).
36. Kim, E.M., Manzar, G. & Zavazava, N. Human iPS cell-derived hematopoietic progenitor cells induce T-cell anergy in in vitro-generated alloreactive CD8(+) T cells. *Blood* **121**, 5167-5175 (2013).
37. Smith, A.M. et al. The transcription factor PU.1 is critical for viability and function of human brain microglia. *Glia* **61**, 929-942 (2013).
38. Feng, R. et al. PU.1 and C/EBPalpha/beta convert fibroblasts into macrophage-like cells. *Proc Natl Acad Sci U S A* **105**, 6057-6062 (2008).
39. Ford, A.L., Goodsall, A.L., Hickey, W.F. & Sedgwick, J.D. Normal adult ramified microglia separated from other central nervous system macrophages by flow cytometric sorting. Phenotypic differences defined and direct ex vivo antigen presentation to myelin basic protein-reactive CD4+ T cells compared. *J Immunol* **154**, 4309-4321 (1995).
40. Pirzgalska, R.M. et al. Sympathetic neuron-associated macrophages contribute to obesity by importing and metabolizing norepinephrine. *Nat Med* **23**, 1309-1318 (2017).

41. Goldmann, T. et al. Origin, fate and dynamics of macrophages at central nervous system interfaces. *Nat Immunol* **17**, 797-805 (2016).
42. Hasselmann, J. et al. Development of a Chimeric Model to Study and Manipulate Human Microglia In Vivo. *Neuron* **103**, 1016-1033 e1010 (2019).
43. Eriksdotter-Nilsson, M., Bjorklund, H. & Olson, L. Laminin immunohistochemistry: a simple method to visualize and quantitate vascular structures in the mammalian brain. *J Neurosci Methods* **17**, 275-286 (1986).
44. Raj, D.D. et al. Priming of microglia in a DNA-repair deficient model of accelerated aging. *Neurobiol Aging* **35**, 2147-2160 (2014).
45. Lawson, L.J., Perry, V.H., Dri, P. & Gordon, S. Heterogeneity in the distribution and morphology of microglia in the normal adult mouse brain. *Neuroscience* **39**, 151-170 (1990).
46. Marsh, S.E. et al. The adaptive immune system restrains Alzheimer's disease pathogenesis by modulating microglial function. *Proc Natl Acad Sci U S A* **113**, E1316-1325 (2016).
47. Hanisch, U.K. & Kettenmann, H. Microglia: active sensor and versatile effector cells in the normal and pathologic brain. *Nat Neurosci* **10**, 1387-1394 (2007).
48. Colonna, M. & Butovsky, O. Microglia Function in the Central Nervous System During Health and Neurodegeneration. *Annu Rev Immunol* **35**, 441-468 (2017).
49. Weinhard, L. et al. Microglia remodel synapses by presynaptic trogocytosis and spine head filopodia induction. *Nat Commun* **9**, 1228 (2018).
50. DeFalco, T., Bhattacharya, I., Williams, A.V., Sams, D.M. & Capel, B. Yolk-sac-derived macrophages regulate fetal testis vascularization and morphogenesis. *Proc Natl Acad Sci U S A* **111**, E2384-2393 (2014).
51. Paolicelli, R.C. et al. Synaptic pruning by microglia is necessary for normal brain development. *Science* **333**, 1456-1458 (2011).
52. Schafer, D.P. & Stevens, B. Microglia Function in Central Nervous System Development and Plasticity. *Cold Spring Harb Perspect Biol* **7**, a020545 (2015).
53. Li, Q.Y. et al. Developmental Heterogeneity of Microglia and Brain Myeloid Cells Revealed by Deep Single-Cell RNA Sequencing. *Neuron* **101**, 207-+ (2019).
54. Zlokovic, B.V. The blood-brain barrier in health and chronic neurodegenerative disorders. *Neuron* **57**, 178-201 (2008).
55. da Fonseca, A.C. et al. The impact of microglial activation on blood-brain barrier in brain diseases. *Front Cell Neurosci* **8**, 362 (2014).
56. Dudvarski Stankovic, N., Teodorczyk, M., Ploen, R., Zipp, F. & Schmidt, M.H.H. Microglia-blood vessel interactions: a double-edged sword in brain pathologies. *Acta neuropathologica* **131**, 347-363 (2016).
57. Zhang, Y. et al. Purification and Characterization of Progenitor and Mature Human Astrocytes Reveals Transcriptional and Functional Differences with Mouse. *Neuron* **89**, 37-53 (2016).
58. Dulken, B.W., Leeman, D.S., Boutet, S.C., Hebestreit, K. & Brunet, A. Single-Cell Transcriptomic Analysis Defines Heterogeneity and Transcriptional Dynamics in the Adult Neural Stem Cell Lineage. *Cell Rep* **18**, 777-790 (2017).
59. Tkachev, D. et al. Oligodendrocyte dysfunction in schizophrenia and bipolar disorder. *Lancet* **362**, 798-805 (2003).

60. Lee, J., Gravel, M., Zhang, R., Thibault, P. & Braun, P.E. Process outgrowth in oligodendrocytes is mediated by CNP, a novel microtubule assembly myelin protein. *The Journal of cell biology* **170**, 661-673 (2005).
61. Wang, S. et al. Human iPSC-derived oligodendrocyte progenitor cells can myelinate and rescue a mouse model of congenital hypomyelination. *Cell Stem Cell* **12**, 252-264 (2013).
62. Liu, M.L. et al. Small molecules enable neurogenin 2 to efficiently convert human fibroblasts into cholinergic neurons. *Nat Commun* **4**, 2183 (2013).
63. Sherriff, F.E., Bridges, L.R., Gentleman, S.M., Sivaloganathan, S. & Wilson, S. Markers of axonal injury in post mortem human brain. *Acta neuropathologica* **88**, 433-439 (1994).
64. Bergsland, M., Werme, M., Malewicz, M., Perlmann, T. & Muhr, J. The establishment of neuronal properties is controlled by Sox4 and Sox11. *Genes Dev* **20**, 3475-3486 (2006).
65. Fuzik, J. et al. Integration of electrophysiological recordings with single-cell RNA-seq data identifies neuronal subtypes. *Nat Biotechnol* **34**, 175-183 (2016).
66. Sweeney, M.D., Kisler, K., Montagne, A., Toga, A.W. & Zlokovic, B.V. The role of brain vasculature in neurodegenerative disorders. *Nat Neurosci* **21**, 1318-1331 (2018).
67. Bostrom, K.I. Cell differentiation in vascular calcification. *Z Kardiol* **89 Suppl 2**, 69-74 (2000).
68. Marques, F. et al. Lipocalin 2 is a choroid plexus acute-phase protein. *J Cereb Blood Flow Metab* **28**, 450-455 (2008).
69. Marques, F. et al. Transcriptome signature of the adult mouse choroid plexus. *Fluids Barriers CNS* **8**, 10 (2011).
70. Arneson, D. et al. Single cell molecular alterations reveal target cells and pathways of concussive brain injury. *Nat Commun* **9**, 3894 (2018).
71. Daneman, R. et al. The mouse blood-brain barrier transcriptome: a new resource for understanding the development and function of brain endothelial cells. *PLoS One* **5**, e13741 (2010).
72. Tremblay, R., Lee, S. & Rudy, B. GABAergic Interneurons in the Neocortex: From Cellular Properties to Circuits. *Neuron* **91**, 260-292 (2016).
73. Hu, J.S. et al. Coup-TF1 and Coup-TF2 control subtype and laminar identity of MGE-derived neocortical interneurons. *Development* **144**, 2837-2851 (2017).
74. Pan, J.Z. et al. Cytokine activity contributes to induction of inflammatory cytokine mRNAs in spinal cord following contusion. *J Neurosci Res* **68**, 315-322 (2002).
75. Feghali, C.A. & Wright, T.M. Cytokines in acute and chronic inflammation. *Front Biosci* **2**, d12-26 (1997).
76. Turner, M.D., Nedjai, B., Hurst, T. & Pennington, D.J. Cytokines and chemokines: At the crossroads of cell signalling and inflammatory disease. *Biochim Biophys Acta* **1843**, 2563-2582 (2014).
77. Yamamizu, K. et al. In Vitro Modeling of Blood-Brain Barrier with Human iPSC-Derived Endothelial Cells, Pericytes, Neurons, and Astrocytes via Notch Signaling. *Stem Cell Reports* **8**, 634-647 (2017).
78. Ormel, P.R. et al. Microglia innately develop within cerebral organoids. *Nat Commun* **9**, 4167 (2018).
79. Masuda, T. et al. Spatial and temporal heterogeneity of mouse and human microglia at single-cell resolution. *Nature* **566**, 388-392 (2019).
80. Wolf, S.A., Boddeke, H.W. & Kettenmann, H. Microglia in Physiology and Disease. *Annu Rev Physiol* **79**, 619-643 (2017).

81. Butovsky, O. & Weiner, H.L. Microglial signatures and their role in health and disease. *Nat Rev Neurosci* **19**, 622-635 (2018).
82. Blakemore, W.F. & Franklin, R.J. Remyelination in experimental models of toxin-induced demyelination. *Curr Top Microbiol Immunol* **318**, 193-212 (2008).
83. Masuda, T. et al. Spatial and temporal heterogeneity of mouse and human microglia at single-cell resolution. *Nature* **566**, 388-392 (2019).
84. Kwan, K.Y. et al. Species-dependent posttranscriptional regulation of NOS1 by FMRP in the developing cerebral cortex. *Cell* **149**, 899-911 (2012).
85. Kraushar, M.L. et al. Temporally defined neocortical translation and polysome assembly are determined by the RNA-binding protein Hu antigen R. *Proc Natl Acad Sci U S A* **111**, E3815-3824 (2014).
86. Ito, R., Takahashi, T. & Ito, M. Humanized mouse models: Application to human diseases. *J Cell Physiol* **233**, 3723-3728 (2018).
87. Askew, K. et al. Coupled Proliferation and Apoptosis Maintain the Rapid Turnover of Microglia in the Adult Brain. *Cell Rep* **18**, 391-405 (2017).
88. Tay, T.L. et al. A new fate mapping system reveals context-dependent random or clonal expansion of microglia. *Nat Neurosci* **20**, 793-803 (2017).
89. Reu, P. et al. The Lifespan and Turnover of Microglia in the Human Brain. *Cell Rep* **20**, 779-784 (2017).
90. Windrem, M.S. et al. A competitive advantage by neonatally engrafted human glial progenitors yields mice whose brains are chimeric for human glia. *J Neurosci* **34**, 16153-16161 (2014).
91. Xu, R. et al. Reversing Abnormal Neural Development by Inhibiting OLIG2 in Down Syndrome Human iPSC Brain Organoids and Neuronal Mouse Chimeras. *BioRxiv* (2018).
92. McQuade, A. et al. Development and validation of a simplified method to generate human microglia from pluripotent stem cells. *Mol Neurodegener* **13**, 67 (2018).
93. Mancuso, R. et al. Stem cell derived human microglia transplanted in mouse brain to study genetic risk of Alzheimer's Disease. *bioRxiv https://doi.org/10.1101/562561*, 562561 (2019).
94. Stevens, B. et al. The classical complement cascade mediates CNS synapse elimination. *Cell* **131**, 1164-1178 (2007).
95. Cunningham, C.L., Martinez-Cerdeno, V. & Noctor, S.C. Microglia regulate the number of neural precursor cells in the developing cerebral cortex. *J Neurosci* **33**, 4216-4233 (2013).
96. Thion, M.S., Ginhoux, F. & Garel, S. Microglia and early brain development: An intimate journey. *Science* **362**, 185-189 (2018).
97. Elmore, M.R. et al. Colony-stimulating factor 1 receptor signaling is necessary for microglia viability, unmasking a microglia progenitor cell in the adult brain. *Neuron* **82**, 380-397 (2014).
98. Gowing, G., Vallieres, L. & Julien, J.P. Mouse model for ablation of proliferating microglia in acute CNS injuries. *Glia* **53**, 331-337 (2006).
99. Lan, P., Tonomura, N., Shimizu, A., Wang, S. & Yang, Y.G. Reconstitution of a functional human immune system in immunodeficient mice through combined human fetal thymus/liver and CD34+ cell transplantation. *Blood* **108**, 487-492 (2006).
100. Slukvin, II Hematopoietic specification from human pluripotent stem cells: current advances and challenges toward de novo generation of hematopoietic stem cells. *Blood* **122**, 4035-4046 (2013).

101. Chen, C. et al. Role of astroglia in Down's syndrome revealed by patient-derived human-induced pluripotent stem cells. *Nat Commun* **5**, 4430 (2014).
102. Muller, F.J. et al. A bioinformatic assay for pluripotency in human cells. *Nat Methods* **8**, 315-317 (2011).
103. Fulmer, C.G. et al. Astrocyte-derived BDNF supports myelin protein synthesis after cuprizone-induced demyelination. *J Neurosci* **34**, 8186-8196 (2014).
104. Marques, S. et al. Oligodendrocyte heterogeneity in the mouse juvenile and adult central nervous system. *Science* **352**, 1326-1329 (2016).
105. Butler, A. & Satija, R. Integrated analysis of single cell transcriptomic data across conditions, technologies, and species. *bioRxiv*, 164889 (2017).
106. Macosko, E.Z. et al. Highly Parallel Genome-wide Expression Profiling of Individual Cells Using Nanoliter Droplets. *Cell* **161**, 1202-1214 (2015).
107. Satija, R., Farrell, J.A., Gennert, D., Schier, A.F. & Regev, A. Spatial reconstruction of single-cell gene expression data. *Nat Biotechnol* **33**, 495-502 (2015).
108. Gentleman, R.C. et al. Bioconductor: open software development for computational biology and bioinformatics. *Genome Biol* **5**, R80 (2004).
109. Butler, A., Hoffman, P., Smibert, P., Papalexi, E. & Satija, R. Integrating single-cell transcriptomic data across different conditions, technologies, and species. *Nat Biotechnol* **36**, 411-420 (2018).
110. Hart, R.P. Strategies for Integrating Single-Cell RNA Sequencing Results With Multiple Species. *bioRxiv*, 671115 (2019).
111. Reimand, J. et al. g:Profiler-a web server for functional interpretation of gene lists (2016 update). *Nucleic Acids Res* **44**, W83-89 (2016).
112. Kim, D., Langmead, B. & Salzberg, S.L. HISAT: a fast spliced aligner with low memory requirements. *Nature methods* **12**, 357-360 (2015).
113. Love, M.I., Huber, W. & Anders, S. Moderated estimation of fold change and dispersion for RNA-seq data with DESeq2. *Genome Biol* **15**, 550 (2014).
114. Pasca, A.M. et al. Functional cortical neurons and astrocytes from human pluripotent stem cells in 3D culture. *Nat Methods* **12**, 671-678 (2015).
115. Liu, Y., Jiang, P. & Deng, W. OLIG gene targeting in human pluripotent stem cells for motor neuron and oligodendrocyte differentiation. *Nat Protoc* **6**, 640-655 (2011).
116. Young, K. & Morrison, H. Quantifying Microglia Morphology from Photomicrographs of Immunohistochemistry Prepared Tissue Using ImageJ. *J Vis Exp* (2018).